23rd Century surprises: Long-term dynamics of the climate and carbon cycle under both high and net negative emissions scenarios

Charles D. Koven[1], Vivek K. Arora[2], Patricia Cadule[3], Rosie A. Fisher[4,5,6], Chris D. Jones[7], David M. Lawrence[4], Jared Lewis[8], Keith Lindsey[4], Sabine Mathesius[9], Malte Meinshausen[8,10], Michael Mills[4], Zebedee Nicholls[8,10], Benjamin M. Sanderson[4,5], Neil C. Swart[2], William R. Wieder[4,11], Kirsten Zickfeld[9]

[1]Climate and Ecosystem Sciences Division, Lawrence Berkeley National Laboratory, Berkeley, California, USA
[2]Canadian Centre for Climate Modelling and Analysis, Environment and Climate Change Canada, University of Victoria, Victoria, British Columbia, Canada
[3]IPSL, CNRS, Sorbonne Université, Paris, France
[4]Climate and Global Dynamics Laboratory, National Center for Atmospheric Research, Boulder, Colorado, USA
[5]Centre Européen de Recherche et de Formation Avancée en Calcul Scientifique, (CERFACS), Toulouse, France
[6]Évolution & Diversité Biologique, University of Toulouse Paul Sabatier III, Toulouse, France.
[7]Met Office Hadley Centre, Exeter, UK
[8]Climate and Energy College, School of Geography, Earth and Atmospheric Sciences, The University of Melbourne, Parkville, Victoria, Australia
[9]Department of Geography, Simon Fraser University, Burnaby, British Columbia, Canada
[10]Climate Resource, Victoria, Australia
[11]Institute of Arctic and Alpine Research, University of Colorado, Boulder, Colorado, USA

Correspondence to: Charles Koven (cdkoven@lbl.gov)

Abstract. Future climate projections from Earth system models (ESMs) typically focus on the timescale of this century. We use a set of four ESMs and one Earth system model of intermediate complexity (EMIC) to explore the dynamics of the Earth's climate and carbon cycles under contrasting emissions trajectories beyond this century, to the year 2300. The trajectories include a very high emissions, unmitigated fossil-fuel driven scenario, as well as a second mitigation scenario that diverges from the first scenario after 2040 and features an 'overshoot', followed by stabilization of atmospheric CO_2 concentrations by means of large net-negative CO_2 emissions. In both scenarios, and for all models considered here, the terrestrial system switches from being a net sink to either a neutral state or a net source of carbon, though for different reasons and centered in different geographic regions, depending on both the model and the scenario. The ocean carbon system remains a sink, albeit weakened by climate-carbon feedbacks, in all models under the high emissions scenario, and switches from sink to source in the overshoot scenario. The global mean temperature anomaly generally follows the trajectories of cumulative carbon emissions, except that 23rd-century warming continues after the cessation of carbon emissions in several models, both in the high emissions scenario and in one model in the overshoot scenario. While ocean carbon cycle responses qualitatively agree both in globally integrated and zonal-mean dynamics in both scenarios, the land models qualitatively disagree in zonal-mean dynamics, in the relative roles of vegetation and soil in driving C fluxes, in the response of the sink to CO_2, and in the timing of the sink-source transition, particularly in the high emissions scenario. The lack of agreement among land models on the

mechanisms and geographic patterns of carbon cycle feedbacks, alongside the potential for lagged physical climate dynamics to cause warming long after CO_2 concentrations have stabilized, point to the possibility of surprises in the climate system beyond the 21st century time horizon, even under relatively mitigated global warming scenarios, which should be taken into

40 consideration when setting global climate policy.

1. Introduction

Climate change is characterized by long timescales, associated with the accumulation of carbon in the atmosphere and other reservoirs of the Earth system due to emissions of CO_2 by anthropogenic activities, and the response of the climate system to the accumulated atmospheric CO_2 burden. The long lifetime of CO_2 in the atmosphere and the proportionality between global

45 warming and long-term cumulative CO_2 emissions are central features of the dynamics of the climate system (Matthews et al., 2009; Allen et al., 2009). These features underlie the widely used policy framework that proposes a 'budget' of remaining carbon emissions that would enable the climate system to remain below a given temperature (Rogelj et al., 2019). Future transient climate change scenarios using comprehensive Earth system models (ESMs) have typically focused on the timescale to the end of the 21st century, in order to inform near-term policy actions that may mitigate climate change. This end date of

50 2100 for these simulations has remained fixed, even though over 30 years have elapsed since the first IPCC assessment (IPCC, 1990).The start date of future scenarios has accordingly progressed from 1990 to 2015, shortening the length of these scenarios. Longer-term dynamics have been explored mainly using Earth system models of intermediate complexity (EMICs) (Zickfeld et al., 2013) and climate system emulators (Meinshausen et al., 2011, 2020; Nicholls et al., 2020b), which allow exploring such dynamics without the computational costs of resolving the full physical and biogeochemical dynamics of an ESM. EMICs

55 (and even more so emulators) typically represent land and ocean biogeochemical processes relevant to the long-term carbon cycle with less detail than comprehensive Earth system models, and so risk missing critical interactions and feedbacks. In contrast, ESMs have prioritized representing processes relevant on timescales to 2100, and may exclude or simplify processes important on longer timescales, such as permafrost carbon feedbacks on land, or sediment biogeochemistry in the ocean.

60 Initial studies using ESMs on this longer time horizon suggest that the proportionality of warming to carbon emissions that is both historically observed and projected on shorter timescales also holds on multi-century timescales, in unmitigated high-end warming scenarios (Randerson et al., 2015; Tokarska et al., 2016). It is less clear whether these relationships hold under mitigated or overshoot scenarios, where net negative carbon emissions are assumed later in the scenario, but the expectation is that the proportional relationship holds for negative carbon emission as well (Zickfeld et al., 2016). Simple models show

65 that the existence of a cumulative emissions to warming proportionality in such scenarios is sensitive to the response timescales of physical and biogeochemical feedbacks in the Earth system (Sanderson, 2020). Existing experiments using ESMs and EMICs suggest that during a positive emissions phase, marine and terrestrial carbon cycles tend to absorb some fraction of added CO_2. During a removal phase, however, they tend to release CO_2 and thus partially offset the decline in atmospheric

CO_2. As a result, we expect that under a scenario with positive emissions followed by net-negative emissions, warming remains
approximately proportional to cumulative CO_2 emissions, but with an additional delay possible due to lags in the carbon cycle
and thermal response to changing CO_2 (Tokarska and Zickfeld, 2015; Jones et al., 2016; Zickfeld et al., 2016; Tokarska et al.,
2019).

To better understand the long-term dynamics of the carbon and climate systems, here we compare a set of four ESMs and one
EMIC under a pair of high emissions and overshoot future climate scenarios that diverge in emissions in the mid-21st century,
and explore the dynamics of carbon and climate under these contrasting trajectories. Further, because these models all report
more detailed information that can allow some degree of process attribution to the dynamics. We thus also explore whether
and where the predicted carbon and climate responses are relatively robust, both within any one model over time and between
scenarios, as well as across models for any given scenario and time period. This allows us to explore where model agreement
does and does not exist, both in the globally integrated response, as well as in the regional and process drivers of that response.
Where ESM or EMIC behavior shows either fundamental disagreement on geographic or process drivers for feedbacks, or
shows global dynamics deviating significantly from the expected linearity between warming and cumulative emissions, we
interpret it as showing a potential for surprises in the future dynamics of the Earth system.

2. Methods

2.1 Scenario Descriptions

All models were forced using the SSP5-8.5 and SSP5-3.4-overshoot scenarios (Riahi et al., 2017; Gidden et al., 2019;
Meinshausen et al., 2020). These scenarios were constructed as part of the CMIP6 set of coordinated experiments for ESMs
(Eyring et al., 2016), and arose out of the ScenarioMIP and SSP design effort (O'Neill et al., 2014, 2016) to cover a wide range
of socioeconomic and policy scenarios and resulting trajectories of greenhouse gas forcings to the Earth system. The simple
extensions beyond 2100 were adapted from those originally conceived in O'Neill (2016), as described in Meinshausen et al.,
(2020). Both of these scenarios follow the SSP5 21st century 'storyline' (Kriegler et al., 2017), which is premised on strong
economic growth, relying largely on fossil fuels in the no-climate-policy baseline. However, they diverge in the year 2040: the
SSP5-8.5 scenario continues on to long-term emissions growth, an 8.5 W m^{-2} anthropogenic greenhouse gas radiative forcing
by 2100, and CO_2 increases until the mid-23rd century. The SSP5-3.4 scenario dramatically changes course in 2040 after
emissions peak, and continues with sustained net-negative CO_2 emissions until the mid-22nd century before stabilizing to near-
zero emissions thereafter; the scale of negative emissions required for this overshoot (>5 PgC/yr for several decades) is much
larger than in the RCP2.6 scenario reported by Jones et al. (2016).

All models were forced with specified atmospheric greenhouse gas concentrations (not greenhouse gas emissions)
(Meinshausen et al., 2020), and land use change forcings (Ma et al., 2020; Hurtt et al., 2020). In a concentration-forced ESM

simulation, the land and ocean carbon cycles respond to the CO_2 concentrations in the atmosphere, which are specified via a global-mean timeseries, but do not feed back on atmospheric CO_2 (Fig. 1a). By integrating the total atmospheric CO_2 reservoir, alongside the prognostic carbon reservoirs on land and ocean, compatible fossil fuel and industrial CO_2 emissions can be calculated to satisfy the conservation of carbon within the Earth system, such that anthropogenic fossil fuel and industrial
105   emissions equal the sum of total changes in land, atmosphere, and ocean carbon stocks (Liddicoat et al., 2020). Land-use-driven carbon emissions are directly reflected in changes in the terrestrial carbon inventories and thus can be separately inferred based on terrestrial model dynamics themselves. Because of differences in carbon cycle feedbacks and in the representation of land use fluxes, the CO_2 emissions inferred by ESMs to be consistent with a given CO_2 concentration pathway will not generally be equal to the CO_2 emissions that were provided by the IAM community for each scenario (Riahi et al., 2017;
110   Gidden et al., 2019; Meinshausen et al., 2020), as shown below. The reason for this is that the representation of C cycle in ESMs is different from the model (MAGICC7) used to convert the IAM emissions into atmospheric CO_2 concentrations in the first place (Meinshausen et al., 2020).

We apply a seven-year running mean to all global timeseries in order to remove the short-term dynamics and focus on longer-
115   term variability.

2.2 Model Descriptions

Here we use results from four ESMs and one EMIC to explore the responses of the Earth system to the two long term scenarios. The models used here were the only models that had performed and archived the necessary experiments as of the time of writing. The four ESMs, all from the CMIP6 generation of models, are the Canadian Centre for Climate Modelling and
120   Analysis fifth-generation Earth System Model, (CanESM5) (Swart et al., 2019d), Community Earth System Model, version two, Whole Atmosphere Configuration (CESM2-WACCM6) (Danabasoglu et al., 2020), the Institut Pierre Simon Laplace (IPSL) IPSL-CM6A-LR (Boucher et al., 2020), and the U.K. Earth System Model (UKESM1) (Sellar et al., 2019). The EMIC is the University of Victoria Earth System Climate Model, version 2.10 (UVic-ESCM) (Mengis et al., 2020).

125   CanESM5 represents a major update since its predecessor CanESM2 (Arora et al., 2011), which was used in CMIP5, and is described in detail in Swart et al. (2019d). The resolution of CanESM5 (T63 or ~2.8° in the atmosphere and ~1° in the ocean) remains similar to CanESM2, and is at the lower end of the spectrum of CMIP6 models. CanAM5, the atmospheric component of CanESM5, has several improvements relative to its predecessor including changes to clouds, aerosols, radiation, land surface, and lake processes. The land component in CanESM5 is represented using the Canadian Land Surface Scheme
130   (CLASS) and the Canadian Terrestrial Ecosystem Model (CTEM) which simulate the physical and biogeochemical land surface processes, respectively. Together CLASS and CTEM calculate fluxes of water, energy, CO_2, and wetland CH_4 emissions at the land-atmosphere boundary. The introduction of dynamic wetlands and their (purely diagnostic) methane emissions is a new biogeochemical process added since CanESM2. The nitrogen cycle over land is not represented but a

parameterization of photosynthesis down-regulation as CO_2 increases is included. The physical ocean (OPA) and sea-ice
135   (LIM2) components of CanESM5 are based on a customized version of NEMO version 3.4.1. The ocean is configured on the
tripolar ORCA1 C-grid with 45 z-coordinate vertical levels, and a nominal horizontal resolution of 1°, with a refinement to
1/3° near the equator. The ocean carbon cycle is represented using the Canadian Model of Ocean Carbon (CMOC). The
biological component is a simple Nutrient-Phytoplankton-Zooplankton-Detritus (NPZD) model, with fixed Redfield
stoichiometry, and simple parameterizations of iron limitation, nitrogen fixation, and export flux of calcium carbonate.

140

CESM2-WACCM is the whole atmosphere configuration of the CESM2 (Danabasoglu et al., 2020) model. This configuration,
which includes fully interactive stratospheric chemistry and dynamics, was used rather than the standard CESM2 configuration
in order to more fully resolve the stratospheric response to the extreme warming in the SSP5-8.5 extension, as the standard
CESM2 uses a set of atmospheric upper boundary conditions that are violated under the level of warming experienced in the
145   long-term high-emissions scenario. The atmosphere is run at 0.9º x 1.25º resolution, and the ocean with a nominal 1º resolution.
The model includes a full ocean model (Parallel Ocean Program version 2, POP2) with modularized biogeochemistry (Marine
Biogeochemistry Library, MARBL). The land model (Community Land Model, version 5, CLM5) is described in Lawrence
et al. (2019). Briefly, CLM5 includes a large number of changes and updates relative to the CLM4 version used in CESM1,
including: a more detailed nitrogen cycle that allows for dynamic responses of N fixation, plant tissue stoichiometry, and leaf
150   nitrogen allocation to changing nutrient limitations; a detailed crop model and more complete representation of land use;
vertically-resolved soil biogeochemistry that includes permafrost carbon dynamics; acclimation of photosynthesis and plant
respiration to changing temperature; and many others. Because of an artifact in model initialization procedure for soil carbon
in CESM2, which left a set of grid cells in the High Arctic with unrealistically high values, here we apply a mask to exclude
all the grid cells where vegetation productivity was equal to zero during a 100-year period of the preindustrial control
155   simulation. This, alongside other model differences, including snow biases in the coupled model, also had the effect of
reducing the permafrost carbon pool in CESM. Thus, while permafrost dynamics are permitted in CESM2 and CLM5, their
feedback to warming is weaker than in the earlier CLM4.5 model as described in Koven et al. (2015).

IPSL-CM6A-LR (Boucher et al., 2020) is the model which was used by the Institut Pierre-Simon Laplace (IPSL) to run most
160   of the simulations needed in the context of the sixth phase of the Coupled Model Intercomparison Project. This coupled model
includes the atmospheric LMDZ model, version 6A-LR (Hourdin et al., 2020), the ocean circulation NEMO model, version
3.6, (Madec et al., 2017), including sea ice NEMO-LIM3 model and thermodynamics and ocean biogeochemistry PISCES-v2
(Aumont et al., 2015), and the carbon cycle ORCHIDEE model, version 2.0 (Krinner et al., 2005). ORCHIDEE and PISCES
models are coupled to the atmospheric LMDZ model via the OASIS3-MCT coupler (Marti et al., 2010). ORCHIDEE and
165   LMDZ share the same spatial resolution of 2.5° x 1.3°, with the vertical atmospheric resolution being composed of 79 vertical
levels up to 80km high. PISCES uses the eORCA1 quasi-isotropic global tripolar grid of 1°, with an additional refinement of

1/3° in the equatorial region and 75 levels in the vertical direction, with steps from 1 to 10m in the surface up to 200m at the bottom.

170 ORCHIDEE land surface model (version 2.0) does not include full nutrient cycles but does include a downregulation of maximum photosynthetic rates under high CO_2 concentrations. Based on Sellers et al. (1996), a logarithmic function was used for modeling the downregulation, using a reference CO_2 value of 380ppm. Moreover, the photosynthesis is calculated from radiation, soil moisture and temperature. The model includes fifteen PFTs that are grouped into three classes (tall vegetation, short vegetation, and bare ground) for the tiling of the land surface. These PFTs share the same leaf phenology but respond to

175 different individual parameters. ORCHIDEE has an eleven-layer soil hydrology scheme, calculating its budget on a tile-basis to keep the balance in soil moisture distribution. Autotrophic and heterotrophic respiration is finally computed for different pools. Plant, litter and soil carbon pools are estimated on a modelled daily basis, compared to all other budgets, that are calculated every 15min, based on the atmospheric dynamics.

180 PISCES models various plankton types (phytoplankton, micro- and mesozooplankton) as well as the biogeochemical cycles of carbon, and main nutrients (P, N, Fe, and Si), where N, P and Si are the limiting nutrients in the phytoplankton's growth. The model has a fixed C:N:P ratio. Oceanic carbon and nutrients input into the model come from atmospheric deposition, river discharge in coastal regions and sediment transport.

185 UKESM1-0-LL is documented in Sellar et al (2019) and its configuration for CMIP6 simulations, including the ScenarioMIP runs is described in Sellar et al (2020). Land and atmosphere share the same horizontal grid: a regular latitude-longitude grid with 1.25º × 1.875º resolution. There are 85 vertical levels extending to 85km in the stratosphere, and full stratosphere-troposphere atmospheric chemistry is simulated using the UKCA model. The ocean component uses the NEMO dynamical ocean on a nominally 1◦ tripolar grid with 75 vertical levels and an explicit nonlinear free surface.

190 The terrestrial biogeochemistry in UKESM1 is based on the land-surface model JULES (Clark et al., 2011; Best et al., 2011), but with some major enhancements developed for UKESM1. In particular the inclusion of a prognostic nitrogen cycle (Wiltshire et al., 2020) allows representation of limitations to carbon storage due to availability of nutrients. Parameters related to photosynthesis, respiration, and leaf turnover have been updated (Harper et al., 2016). The number of natural PFTs was increased from five to nine to represent the distinction between evergreen and deciduous plants and between tropical and

195 temperate evergreen trees. The new dynamic vegetation and PFTs yield a closer match to observed vegetation distribution, with particular improvements to tropical and boreal forests and the high latitudes (Harper et al., 2018). The land use scheme designates a portion of each gridbox as cropland and a portion as pasture land, where only crops and pasture grasses can grow, respectively, to the exclusion of trees and shrubs. In the remainder of the gridbox, nine natural PFTs compete for space, which determines the distribution of forests, grasslands, shrublands, and bare soil.

200   Ocean biogeochemistry in UKESM1 is represented with the MEDUSA-2 model (The Model of Ecosystem Dynamics, nutrient
Utilisation, Sequestration and Acidification; (Yool et al., 2013)): an intermediate-complexity plankton ecosystem model which
resolves a dual size-structured ecosystem of small (nanophytoplankton and microzooplankton) and large (microphytoplankton
and mesozooplankton) components. It explicitly includes the biogeochemical cycles of nitrogen, silicon, and iron nutrients as
well as the cycles of carbon, alkalinity, and dissolved oxygen.

205   The University of Victoria Earth System Climate Model (UVic ESCM) is a model of intermediate complexity with a horizontal
grid resolution of 1.8˚(meridional) x 3.6˚(zonal). The version of the UVic ESCM used here (version 2.10) is described in detail
in Mengis et al. (2020). UVic ESCM 2.10 includes a 3-D ocean general circulation model coupled to a dynamic-
thermodynamic sea-ice model and a single layer energy-moisture balance model of the atmosphere with dynamical feedbacks.
The land surface model is based on a simplified version of the Hadley Centre's MOSES land-surface scheme. New
210   developments include a representation of soil freeze–thaw processes resolved in 14 subsurface layers (Avis et al., 2011), a
multi-layer representation of soil carbon and soil respiration (MacDougall et al., 2012), and a representation of permafrost
carbon, which is prognostically generated within the model using a diffusion-based scheme meant to approximate the process
of cryoturbation (MacDougall and Knutti, 2016). In addition, the terrestrial component represents vegetation dynamics
including five different plant functional types. The ocean carbon cycle is simulated by means of an OCMIP-type inorganic
215   carbon-cycle model and a new marine ecosystem/biogeochemistry model solving prognostic equations for nutrients,
phytoplankton, zooplankton and detritus (Keller et al., 2012). The new ocean biogeochemistry module includes phytoplankton
light limitation, a more realistic zooplankton growth and grazing model, and an iron limitation scheme to constrain
phytoplankton growth. Sediment processes are represented using an oxic-only calcium-carbonate model. Decadal-average
values of spatially-explicit variables are used for this study.

220   ## 3. Results

3.1 Climate Responses

In the historical and SSP5-8.5 scenario, global mean temperature change relative to the preindustrial (Fig. 1b) increases
monotonically in all models, with a wide range of responses by 2300 from ~18 degrees C in the CanESM5 to ~8 degrees in
the UVic-ESCM model. Here, a notable difference arises between the ESMs and the UVic-ESCM EMIC, with much higher
225   transient warming in the ESMs than in the EMIC. This is at least in part due to a sampling bias related to the set of models that
have performed these long-term scenarios: all four ESMs used here report transient climate response (TCR) greater than 2.4
ºC and a transient climate response to emissions (TCRE) greater than 2 ºC/EgC (mean of 2.16 ºC/EgC) versus the CMIP6
mean of 2.0 ºC TCR and 1.8 ºC/EgC TCRE (Arora et al., 2020); whereas the specific version of UVic-ESCM used here reports
a TCR of 1.8 ºC and a TCRE of 1.8 ºC/EgC (MacDougall et al., 2020), closer to the CMIP6 mean. During the period of CO_2
230   stabilization and decline in the 23rd century, three of the ESMs continue to warm substantially, while in one ESM (UKESM1)

and the EMIC, the global temperature stabilizes. This implies a substantial slow component in the models which continue to warm past the period of CO_2 stabilization, beyond the effective transient values reported above (which reflect short-to-medium term processes that dominate the TCRE) (Proistosescu and Huybers, 2017).

235 In contrast, in the SSP5-3.4-overshoot scenario, global temperatures follow the CO_2 concentration trajectory to first peak and then cool during the 21st century in all models. Subsequent dynamics vary between the models: most stabilize at a cooler temperature than the peak 21st century value, while one model (CESM2-WACCM) reaches a minimum temperature at ~2200, and then resumes warming, albeit at a slower rate, during the 23rd century. As in the very high emissions scenario, there is a separation in the amount of warming between the relatively less sensitive EMIC and more sensitive ESMs both at the peak
240 and in the subsequent overshoot and stabilization period.

3.2 Carbon Cycle Responses

Responses of the globally-integrated terrestrial and marine carbon cycle to the two scenarios for all models are shown in fig. 1c-d. Under both the SSP5-8.5 and SSP5-3.4-overshoot scenario, the terrestrial carbon cycle (Fig 1c) in all models shifts at some point from being a net sink of carbon from the atmosphere to a neutral or net source of carbon to the atmosphere. In the
245 SSP5-8.5 scenario, the timing of this transition varies widely between models, from ~2100 in UVic-ESCM to ~2220 in CESM2-WACCM. The magnitude of the carbon fluxes also varies widely between models, with CanESM5 showing strongest terrestrial uptake, peaking around 2100, and then reversing to become the strongest terrestrial source out of the models examined here during the 23rd century.

250 Overall, the pattern of terrestrial sink-to-source transition under long-term high emissions is qualitatively consistent with the results of Tokarska et al. (2016), which show a similar transition in all of the models examined in the RCP8.5 extension experiment. This pattern follows from the dynamics described by Randerson et al. (2015) whereby terrestrial carbon-climate feedbacks strengthen over time, at the same time that the terrestrial carbon-concentration feedbacks weaken, although the experimental protocol followed here, which does not separate CO_2 climate and physical effects as in (Arora et al., 2020), does
255 not allow this feedback decomposition to be performed.

For the SSP5-3.4-overshoot scenario, model agreement of the terrestrial carbon cycle is much higher, with all models transitioning from sink to source during the late 21st or early 22nd centuries, which counteracts some of the net-negative anthropogenic emissions by that time in terms of their effect on lowering atmospheric CO_2 concentrations, and consistent with
260 the CMIP5 RCP2.6 results shown in Jones et al. (2016). The timing of the biospheric switch from sink to source follows by decades the change in the sign of CO_2 emissions from net positive to net negative. All of the models then revert to a roughly carbon-neutral terrestrial biosphere during the 23rd century. Notably, models across the ensemble show a reduced range of variation in the magnitude of carbon fluxes for the SSP5-3.4-overshoot scenario, relative to the SSP5-8.5 scenario.

265   Over ocean (Fig 1d), inter-model agreement is in general much higher than over land, although ensemble spread does increase beyond 2100 in the SSP5-8.5 scenario. Peak carbon uptake for both scenarios occurs prior to 2100 in all models, with an earlier and smaller-magnitude peak in the SSP5-3.4-overshoot than the SSP5-8.5 scenario. In the models, the ocean carbon uptake then gradually weakens but remains positive through the 22nd and 23rd centuries in the SSP5-8.5 scenario, while in the SSP5-3.4-overshoot scenario, uptake rapidly reverses to become a source through most of the 22nd century (lagging behind the

270   change in the sign of net CO_2 emissions by decades), before then reversing again in the late 22nd century to become a weak sink again through the remainder of the scenario.

3.3 Diagnosed CO_2 Emissions

Annual (fig. 2a) and cumulative (fig. 2b) CO_2 emissions, which are compatible with the specified CO_2 concentration pathway in these simulations, follow the overall trajectory of the emissions used to generate the concentrations scenario using the

275   MAGICC7 model. The additional spread in ESMs and the UVic EMIC is due to the difference between the models' carbon cycles and the carbon cycle in the MAGICC7 model (section 2.1). Also shown in fig. 2a are the annual fossil-fuel and industrial CO_2 emissions used to generate the two scenarios showing approximate agreement between the compatible emissions diagnosed from the ESM and EMICs.

280   In the SSP5-8.5 scenario, the model ensemble spread in compatible emissions is widest at the end of the 21st century when emissions also peak, and declines during the 22nd century. In one model under SSP5-8.5 (CanESM5), negative emissions are required in the 23rd century to balance the strong and sustained terrestrial carbon source active at that time in that scenario, whereas in the rest of the models slightly positive or roughly zero emissions are inferred for the scenario. In the SSP5-3.4-overshoot scenario, the ensemble spread in compatible emissions peaks first at the time of peak positive CO_2 emissions, and

285   then increases again during the period of strongest negative CO_2 emissions, as models disagree on the magnitude of carbon cycle responses to each of these phases.

The shape of the cumulative diagnosed CO_2 emissions (fig. 2b) roughly follows the trajectory of the atmospheric CO_2 concentrations shown in fig. 1a. Ensemble spread in cumulative diagnosed CO_2 emissions shows the relative responses of the

290   carbon cycles in each model to positive and negative CO_2 emissions, with, e.g. the IPSL-CM6A-LR model requiring higher cumulative emissions to balance its stronger sink throughout the entirety of the SSP5-3.4-overshoot scenario, and the CanESM5 model requiring higher amounts of cumulative CO_2 emissions to balance its high sink in the SSP5-8.5 scenario until ~2200, when that model's terrestrial system reverses from a strong sink to a strong source.

295   Each of the fluxes, averaged across the models, are shown together in figure 2c-d. Here, for each scenario, the pink line shows the inferred emissions time series, the black line shows the change in atmospheric CO_2, and the accumulation in land (green)

and ocean (blue) are shown by the area of sinks (hatching) or sources (stippling). This shows lags in the land and ocean carbon fluxes in response to changes in emissions, particularly for the SSP5-3.4-overshoot scenario (fig. 2d), where the terrestrial and ocean systems remain sinks for several decades during the period of declining and negative CO_2 emissions, before they switch to become sources, which partially offset the negative emissions. In the SSP5-8.5 scenario, lags are less evident, but the net behavior of the ocean is to at least partially offset the net carbon losses on land during the period after the mid-22nd century.

3.4 Temperature Response to Cumulative Emissions

Plotting global mean temperature change as a function of diagnosed cumulative CO_2 emissions (fig. 3) reproduces the near linear relationship between temperature change and cumulative CO_2 emissions described in (Tokarska and Zickfeld, 2015; Jones et al., 2016; Zickfeld et al., 2016). Note, however, that the temperature change shown here includes the response to non-CO_2 forcings, whereas the linear relationship is strictly defined only for CO_2 (Matthews et al., 2009; Collins et al., 2013), and thus the relationship shown here represents an "effective TCRE" (Matthews et al., 2017) that includes these non-CO_2 forcings. There is some deviation from linearity in the cumulative carbon emissions to temperature relationship in SSP5-8.5 scenario. Initially, up to approximately 2000 PgC, temperature increases less than linearly with cumulative CO_2 emissions. There are two potential explanations for this curvature. The first potential explanation is the role of non-CO_2 forcers, which contribute a larger fraction of the total greenhouse gas forcing in the early than late part of this scenario (Meinshausen et al., 2020). The second potential explanation is lags in the carbon and climate systems relative to emissions. An analysis with CO2-only experiments up to 2100 (Nicholls et al., 2020a) found a similar slight negative curvature as observed here, suggesting that lags in the carbon and climate systems are dominant up to around 2000 PgC. The temperature vs cumulative emissions relationship is approximately linear for cumulative emissions between 2000 PgC and 4000 PgC, except for the UVic ESCM. The less-than-linear relationship in EMICs was noted before and attributed to the saturation of CO_2 radiative forcing at high cumulative emissions (Herrington and Zickfeld, 2014; Tokarska et al., 2016). In the final half-century of the SSP5-8.5 scenario, temperature in the ESMs continues to increase in response to approximately stable radiative forcing. This continued warming reflects the lags in the carbon and thermal response to CO_2 emissions and non-CO_2 forcings. The one EMIC shows a more linear response in this part of the scenario than the ESMs. In the ESMs shown here for the SSP5-8.5 scenario, this lagged-warming tail is larger, particularly in the case of CanESM5, than the corresponding behavior shown in Tokarska et al., (2016).

By breaking the cumulative emissions plots into roughly centennial-length segments, fig 3 shows the dynamics for the two scenarios over time for all of the models. This underscores the continuity of the cumulative emissions curve through the 22nd century in the SSP5-8.5 scenario (fig. 3a), and the break in that relationship for several of the models during the 23rd century. For the SSP5-3.4-overshoot scenario (fig. 3b), the separation by centuries further shows the slight nonlinearity evident in some—but not all—of the models during the peak and initial overshoot period. In the overshoot scenario, there is not a consistent deviation from linearity at the point of overshoot and negative CO_2 emissions. Some models (UVic-ESCM, CanESM5) follow roughly the same trajectory in temperature vs cumulative emissions space in the initial period of negative

330   emissions, while others (IPSL-CM6A-LR, CESM2) follow a lower-temperature trajectory after peak warming, and one model (UKESM1) follows a higher-temperature curve in temperature vs cumulative space after peak emissions. This could be due to different roles of carbon versus thermal inertia in the declining CO_2 phase (Zickfeld et al., 2016). CESM2-WACCM also shows a distinctly different 23rd-century response to the other models, with a significant increase in temperatures in response to near-constant radiative forcing, and nearly zero inferred emissions, over this period.

335   **3.5 Regional variation in carbon and temperature dynamics**

3.5.1 Terrestrial carbon cycle

Aggregated globally, there is some commonality and a large degree of divergence between models across these two contrasting scenarios. While all models show some consistent patterns (e.g., a shift on land from sink to source), individual models also show differing dynamics both in the patterns, the timing, and the magnitudes of the carbon and temperature response. It is

340   possible to disaggregate these dynamics regionally to better understand the mechanistic basis of the carbon and temperature response, and to explore whether any qualitative similarity holds at the more regional scales. We thus focus on zonal-mean trajectories of carbon and temperature as a way to further understand the degree of similarity in results across models and within any model over time and scenarios.

345   Fig. 4 shows zonal-mean terrestrial carbon flux dynamics for the five models and two scenarios over the full historical to future period. The value for a given latitude is the average over all land cells in that latitude, regardless of the fractional coverage of land in grid cells. In the historical and near-future time period that are shared between the scenarios, the five models already show a strong divergence in behavior: CanESM5 projects 21st century carbon sinks in both the tropics and northern high latitudes; CESM2-WACCM has one main sink area in the tropics and a much weaker sink at northern mid and high latitudes;

350   IPSL-CM6A-LR and UKESM1 also have one main sink area, but in the northern mid- and high latitudes, and UVic-ESCM shows a weak sink in the tropics and growing carbon source in the higher latitudes. Over time in the SSP5-8.5 scenario (fig. 4a), each of these models show further divergent results: in CanESM5, both the tropical and northern high latitude regions shift from sinks to sources at roughly the same time, becoming sources by the mid-22nd century; in CESM2-WACCM, the tropics remain a sink through the end of the 22nd century, while the northern high latitudes shift to become a source by the

355   end of the 21st century, with the source peaking during the 22nd century and weakening thereafter; in IPSL-CM6A-LR the northern sink weakens gradually over time to become neutral by the mid-22nd century, while the tropics become a strong source of carbon during the 22nd century; in UK-ESM1, the northern sink is sustained while the tropics shift to become a source, and in UVic-ESCM the northern high latitudes become a strong source and the tropics a weak source. Thus the regionally-disaggregated dynamics show even greater divergence than the global integral, with differing locations—and thus

360   mechanisms—driving the overall shift from sink to source across models. Further, the areas of most active terrestrial carbon cycle dynamics shift from one region to the next across centuries within any one model.

Zonal-mean dynamics are both more muted in magnitude and more similar between models for the SSP5-3.4-overshoot scenario (fig. 4b). In both the CanESM5 and CESM2-WACCM models, the early sinks weaken in favor of a source of carbon

365   in the tropics during the net negative CO_2 emissions period from roughly 2050 to 2150. The IPSL-CM6A-LR and UKESM1 models show similar dynamics, but with a larger overlay of interannual variability. The UVic-ESCM model shows a relative brief but strong loss of carbon from northern high latitudes during the period of peak warming, and a slower and weaker loss of carbon from the tropics during the subsequent period of net negative CO_2 emissions.

370   Further disaggregating the dynamics into zonal-mean vegetation and soil carbon pools (fig. 5) shows even greater divergence between the models. Vegetation carbon pools accumulate in both the tropics and northern mid-high latitudes in the SSP5-8.5 scenario in both CanESM5 and CESM2-WACCM; in IPSL-CM6A-LR, the northern latitudes gain vegetation carbon but the tropical latitudes lose large amounts of vegetation carbon; in UKESM1 vegetation carbon accumulates at mid-high latitudes of both hemispheres but is roughly neutral in the tropics; in UVic-ESCM, northern vegetation is a weak sink and tropical

375   vegetation is roughly neutral. For soils, CanESM5 gains carbon in both the tropical and mid-high latitude belts, albeit with a delay relative to vegetation pools, through the mid 22nd century, but then shifts to lose carbon in soils from both belts by the end of the 23rd century; CESM2-WACCM gains soil carbon through most of the world but also projects substantial carbon losses from the northern high latitude soils beginning in the late 21st century; IPSL-CM6A-LR loses soil carbon, mainly from the tropics, starting mainly during the 22nd century; UKESM1 shows a stronger tropical soil carbon loss and a higher latitude

380   soil carbon gain; and UVic-ESCM shows strong losses of carbon at northern high latitudes and gains of soil carbon in the northern mid-latitudes. Thus, under the SSP5-8.5 scenario, both soil and vegetation dynamics differ markedly across the models, as well as regionally within each model.

For the SSP5-3.4-overshoot scenario, zonal-mean disaggregation of vegetation and soil carbon (fig. 5c-d) shows some greater

385   degree of similarity between model dynamics. All five models agree that northern mid-high latitudes will gain carbon in vegetation. In the tropics, three models (CanESM5, CESM2-WACCM, and IPSL-CM6A-LR) predict that carbon gains in tropical vegetation peak by the end of the 21st century, while UKESM1 predicts sustained tropical vegetation carbon losses from the historical through the end of the scenario, and UVic-ESCM shows more neutral behavior of vegetation globally. CESM2-WACCM and UKESM1 also show substantial losses of vegetation carbon in subtropical ecosystems. For soil carbon

390   dynamics, the patterns are much more muted than in the high-emissions case, with weaker but sustained carbon gains in soils of northern high latitudes in the CanESM5, IPSL-CM6A-LR, and UKESM1 models, and a weaker loss of carbon from northern high latitudes and gain of carbon in the northern mid-latitudes in the CESM2-WACCM model, and for the UVic-ESCM model, northern soil carbon losses are weaker than in the very high emissions case but still stronger than any of the other models.

3.5.2 Ocean carbon cycle

395   Zonal-mean breakdowns of the ocean carbon cycle are much more consistent between models (Fig. 6). All models show near-term sinks in the mid and high latitudes of both hemispheres, with sources in the tropics. Under the SSP5-8.5 scenario, all models show a poleward migration of the Southern Ocean sink, and a weakening followed by a strengthening of the tropical source. In four of the models, the northern mid- and high- latitude sinks weaken during the 22nd century, while they remain strong in the IPSL-CM6A-LR model. While the zonal-mean patterns of the ocean carbon flux are broadly consistent across

400   the models, the magnitudes and meridional extents of the source and sink regions vary significantly, leading to the large spread in net global fluxes across models seen under the SSP5-8.5 scenario (Fig 1d). In the SSP5-3.4-overshoot scenario, all models show roughly similar dynamics: the tropical source strengthens, the northern mid- and high- latitudes sinks weaken, and the southern ocean shifts from sink to source, although differences in the timing, strength and meridional extent of these transitions are again evident between models.

405   ### 3.5.3 Temperature

Regional temperature dynamics are roughly similar between ESMs (Fig. 7). All models show polar amplification, and thus warming proceeds faster at high latitudes, particularly in the northern hemisphere. Under the high emissions scenario, global warming is overwhelming, with >10 degrees C warming at all latitudes and much higher warming at the poles, with warming reaching 10 degrees at the northern polar region within this century in all five models. Under the overshoot scenario, polar

410   amplification is still present in all models, and global warming peaks and then declines and stabilizes after the peak CO_2 period in all models except CESM2-WACCM.

In CESM2-WACCM, for the overshoot scenario, the northern mid- to high latitudes return to almost the preindustrial temperature during the 22nd century, and then subsequently warm again in the 23rd century, despite no further CO_2

415   concentration increases; this area is responsible for the vertical tail to the cumulative emissions-temperature change plot in the 23rd century in that model (Fig. 3b). Plotting the 100-year mean temperature difference between the 23rd and 22nd centuries (fig. 8a), shows that the 23rd century warming in the model is centered on the Northern Atlantic, suggesting a control by Atlantic Meridional Overturning Circulation (AMOC). To explore this hypothesis, we calculate AMOC as the maximum value of the annual-mean meridional mass flow stream function in the Atlantic basin north of 20N, and plot time series of this for

420   all ESMs and scenarios in fig. 8b. This shows that CESM2 AMOC starts out with stronger AMOC than the other ESMs, which partially collapses during the period of warming to reach a minimum at around 2100 and recovers thereafter in the SSP5-3.4-overshoot scenario, with a much stronger rebound than other ESMs considered here. This AMOC recovery response is consistent with earlier long-term overshoot scenarios (Nakashiki et al., 2006) as well as long-term constant 2xCO2 experiments (Manabe and Stouffer, 1994). Thus this supports the interpretation that the AMOC recovery in that model drives the 23rd-

425   century warming. An additional piece of evidence to support the transient shutdown and subsequent recovery of AMOC as

being the key driver of the CESM-WACCM temperature vs cumulative emissions nonlinearity shown here comes from the comparison of Hu et al. (2020) between CESM2 and a closely related model, E3SM. They show that both models have similar ECS but CESM has a substantially lower TCR, which they attribute to its higher sensitivity of AMOC strength to warming. The 23rd century warming in CESM2-WACCM thus appears to reflect an AMOC that is transiently weakened during the 22nd century due to freshwater influx associated with warming, leading to relative cooling around the North Atlantic and throughout the high latitudes, but which then recovers and removes that cooling anomaly that was present during the weakened-AMOC period.

4. Discussion

The concept of proportionality of global warming to cumulative emissions and the related metric of transient climate response to emissions (TCRE) are enormously valuable in understanding the expected response of global temperature change to anthropogenic emissions. At the same time, the utility of this framework is limited by both the persistent spread in TCRE across model ensembles (Arora et al., 2020; Jones et al., 2013), as well as the possibilities of behavior in the coupled climate and carbon cycle systems that may give rise to nonlinear trajectories of temperature as a function of cumulative emissions. The IPCC and UNFCCC framework for climate change policy uses a framework described in (Rogelj et al., 2019). Within this abstraction of the climate system, these nonlinearities take two forms: a zero emission commitment (ZEC), which is any warming which arises after the point that CO_2 emissions reach net zero, and thus would lead to vertical tails (either positive or negative) in the cumulative emissions plots (although part of the tail warming shown here may be in response to near-constant non-CO_2 forcing), and an allowance for Earth system feedbacks that are unrepresented or underrepresented in existing Earth system models and thus not included in the spread of TCRE from ESMs. Physical or biogeochemical lags in the Earth system, beyond those quantified by the ZEC or specifically enumerated as unrepresented feedbacks, are not accounted for in this framework, though the updated framework of Nicholls et al., (2020a) allows for non-linearities between cumulative CO_2 emissions and CO_2-induced warming in remaining carbon budget calculations.

The pair of scenarios explored here bracket a wide range of possible dynamics in the Earth system over the next few centuries, from a high CO_2 concentration world with continuous and overwhelming global warming over the coming centuries to one in which CO_2 is stabilized and reduced following a peak warming during this century (Figs. 1-2). In each of these scenarios, the models studied in general follow the expected linearity in TCRE, before 2200 (Fig. 3). At the same time their internal dynamics vary widely from each other, particularly in the terrestrial carbon cycle and under high levels of global warming, where there is little agreement on the geographic and mechanistic drivers of the terrestrial carbon cycle responses to the warming (Figs. 4-5). Possibly this is due to some degree of tuning (either implicit or explicit) to capture the observed globally-integrated 20th century carbon balance trajectory, a constraint whose influence weakens at regional levels and over time into the future (Hoffman et al., 2014).

The five models used here vary widely in the representation of their terrestrial biospheres: two (UKESM1, and UVic-ESCM)
460   include vegetation dynamics, while the other three (CanESM5, CESM2-WACCM, IPSL-CM6A-LR) use prescribed and static
distributions of plant functional types. Two models (CESM2-WACCM and UVic-ESCM) include the dynamics of deep and
frozen soil carbon, while the others drive soil biogeochemistry using near-surface soil temperatures and thus exclude the
possibility of permafrost carbon feedbacks to climate change. Two models (CESM2-WACCM and UKESM1) include the
nitrogen cycle on land, while the others do not. While there does not appear to be a general signature associated with the
465   inclusion of vegetation dynamics or nitrogen here, the inclusion of permafrost carbon in both models here does lead to a
signature of large soil carbon losses at high latitudes under the high-warming scenario. Overall, the models differ widely in
the aggregated magnitude of their responses to climate and elevated CO_2 (Arora et al., 2020). The structural differences likely
underlie the diversity of global and regional responses, although given the myriad structural and parametric differences
between the models it is not possible to attribute the dynamics in a more rigorous way (Fisher and Koven, 2020), nor is it
470   possible with the limited sample size considered here to assess whether model agreement in shorter term response arises due
to common representation of relevant processes or calibration constraints imposed by historical global carbon-climate
dynamics. Nonetheless, the diverse potential for global and regional carbon cycle dynamics to change sign under these
scenarios highlights the continued need for improved comprehension of the major drivers of terrestrial carbon cycle dynamics.

475   The ocean carbon cycles of the models, and the thermal response of the climate system to greenhouse gas forcing, in general
shows better qualitative agreement with each other (Figs. 1c, 6), but again ensemble spread increases after the 21st century in
the high-emission scenario, and other surprises may be in store. In particular, two distinct types of lags in the physical system
may lead to further warming beyond the time period in which greenhouse gases increase: if carbon emissions cease without
overshoot, lags in the physical climate may lead to continued warming after cessation, while in the overshoot case, mechanisms
480   such as AMOC slowdown may temporarily obscure some of the warming, but then upon recovery of AMOC this temporary
regional cooling may dissipate, leading to a resumption of warming long after the CO_2 has stabilized (fig. 8). If such dynamics
are real features of the Earth system, this would be of critical concern — even if we deploy large negative emissions, we still
would have to have a plan for a world in which all they do is stabilise, rather than reduce, temperatures. Of particular note is
that CESM2 showed a negative zero emission commitment in (MacDougall et al., 2020), despite showing the large 23rd-
485   century warming with near-zero inferred emissions in the overshoot and stabilization scenario here, indicating that the ZEC
framework as currently defined by MacDougall et al. (2020) as the temperature change evaluated 50 years following net-zero
emissions may be insufficient for quantifying such lagged effects of CO_2 on climate. Further, we note that CESM2 shows the
highest effective ECS of any of the models whose transient climate response is within the "likely range" as constrained by
observed warming trends (Nijsse et al., 2020), and thus underscores the possibility for nonlinearities in temperature versus
490   cumulative emissions unless behavior can also be constrained by paleoclimate evidence (Sanderson, 2020; Tierney et al.,
2020).

Given that the plant-physiological and other CO_2 concentration-dependant processes represented in models are not routinely tested against observations from the highly out-of-sample conditions experienced under each of these scenarios (e.g. very high

495   atmospheric CO_2 concentrations under SSP5-8.5 or rapidly decreasing CO_2 concentrations under SSP5-3.4-overshoot), it is to be expected that model differences will be large. Despite this, it is important to note that the ensemble spread in compatible emissions, which include all these uncertain carbon-cycle feedbacks, is relatively small when compared to the mean magnitude of the emissions themselves, particularly under the overshoot scenario (fig. 2a-b). Thus the uncertainty associated with carbon cycle feedbacks is relatively small compared to the anthropogenic emissions themselves. Further, the uncertainty does not

500   conflict with the central result that warming is roughly proportional to cumulative emissions, at least for this century and the following one, and these results support the need for rapid reductions in CO_2 emissions to prevent the extreme impacts associated with warming.

Nonetheless, these results also suggest that there may be longer-term surprises in the coupled climate-carbon system to be

505   encountered both in high-emissions and overshoot warming scenarios. The evident lack of consistent predictions in the terrestrial models, combined with the known structural differences, and the fact that none of the models include a complete set of processes that may be considered likely to affect the terrestrial carbon cycle, support the approach of budgeting for feedbacks present in the Earth system but not included in ESMs, at least until greater convergence in terrestrial carbon cycle models can be shown. The ocean carbon cycle as well shows greater uncertainty on this time horizon than on the pre-2100

510   dynamics, for which there is greater agreement. The wide range of results shown here, despite a small number of models analyzed, also underscore the need for further testing of model dynamics on these longer timescales, the inclusion of more models and more systematic exploration of parameter and structural uncertainty on these longer-term dynamics, as well as the identification and use of observational constraints that are relevant to these longer-term dynamics of the coupled carbon and climate systems. At the same time, unanticipated physical dynamics, such as the transient weakened-AMOC-driven cooling

515   and its subsequent reversal may also be relevant on long timescales. Thus, we should continue to anticipate that surprises in the long timescale climate response are possible, even under relatively mitigated global warming scenarios, and which should be taken into consideration when setting global climate policy.

5. Conclusions

520   We examine four CMIP6 ESMs, alongside a reduced-complexity EMIC, in a pair of experiments that extend to the year 2300, to explore the dynamics of the coupled carbon and climate systems on this timescale, which is longer than those typically considered in ESM analysis. We show that under contrasting high-emissions and overshoot scenarios warming is approximately proportional to total cumulative CO_2 emissions, but also that distinct deviations from linearity arise in some of

525 the ESMs on post-2200 timescales. These deviations underscore the limits to our ability to coherently project the dynamics of the Earth system on these longer timescales. We note that, as on shorter timescales, the projections of terrestrial carbon dynamics differ most strongly between models, and that on the longer timescales there is still enormous uncertainty in projected carbon dynamics. This uncertainty is evident in multiple ways: between the model projections of global carbon changes; between the model projections of the geographical regions contributing to feedbacks; between the pools responsible for the basic mechanisms of carbon cycle variability; and between one century to the next within models. We also show that lagged

530 temperature effects leading to warming after cessation or reversal of emissions, beyond what has been shown in earlier or simpler models, may be possible outcomes in these projections. These results show that a greater emphasis on identifying, attributing, and reducing uncertainty is needed on the wider range of possible futures that can be explored on these longer timescales, and that until such uncertainty can be reduced, we must anticipate and allow for surprises such as these in formulating global climate policy over these longer timescales.

535 **Data Availability**

All CMIP6 data is available on the Earth system grid. IPSL-CM6A-LR output is available at: (Boucher et al., 2018, 2019b, a); CESM2-WACCM data available at: (Danabasoglu, 2019c, b, a); CanESM5 data available at: (Swart et al., 2019b, c, a); UKESM data available at: (Tang et al., 2019; Good et al., 2019a, b). UVic-ESCM output is available at (Mathesius and Zickfeld, 2021). All analysis code is available as a jupyter notebook at

540 https://github.com/ckoven/longterm_carboncycle/blob/master/longterm_carboncycle.ipynb

Author Contributions

C.K. and K.Z. conceived of study, with contributions from D.L.. All authors contributed to the design and/or use of one of the ESMs, EMIC, or long-term scenarios used in the analysis (CESM2-WACCM: C.K., R.F., D.L., K.L., M. Mills, B.S., W.W.; CanESM5: V.A., N.S.; IPSL-CM6A-LR: P.C.; UKESM1: C.J.; UVic-ESCM: S.M., K.Z.; long-term scenarios: J.L., M.

545 Meinshausen, Z.N.). C.K. performed data analysis and visualizations, with contributions from C.J., S.M., and K.Z.. C.K. wrote the initial manuscript draft. All authors provided input and feedback to manuscript text and figures, with particularly significant contributions from V.A., P.C., R.F., C.J., D.L., M. Meinshausen, Z.N., B.S., W.W., and K.Z..

Competing Interests

The authors declare that they have no conflict of interest.

550 **Acknowledgements**

C.K. was supported by the Director, Office of Science, Office of Biological and Environmental Research of the U.S. Department of Energy under Contract DE-AC02-05CH11231 through the Early Career Research Program, the Regional and Global Model Analysis Program (RUBISCO SFA), and the Next Generation Ecosystem Experiment-Tropics (NGEE-Tropics) project. R.F. was also supported by NGEE-tropics. W.W., D.L. and R.F. were supported by the National Center for

555 Atmospheric Research, which is sponsored by the U.S. National Science Foundation, which is a major facility sponsored by the National Science Foundation under cooperative agreement 1852977. Computing resources (doi:10.5065/D6RX99HX) were provided by the Climate Simulation Laboratory at NCAR's Computational and Information Systems Laboratory, sponsored by the National Science Foundation and other agencies. W.W. was supported by the U.S. Department of Agriculture NIFA award 2015-67003-23485 and NASA Interdisciplinary Science Program award number NNX17AK19G. Benjamin

560 Sanderson is funded by the French National Research Agency, project no. ANR-17-MPGA-0016. C.D.J. was supported by the Joint UK BEIS/Defra Met Office Hadley Centre Climate Programme (GA01101) and the European Union's Horizon 2020 research and innovation programme CRESCENDO (grant agreement No 641816). We acknowledge the World Climate Research Programme, which, through its Working Group on Coupled Modelling, coordinated and promoted CMIP6. We thank the climate modeling groups for producing and making available their model output, the Earth System Grid Federation (ESGF)

565 for archiving the data and providing access, and the multiple funding agencies who support CMIP6 and ESGF.

References

Allen, M. R., Frame, D. J., Huntingford, C., Jones, C. D., Lowe, J. A., Meinshausen, M., and Meinshausen, N.: Warming caused by cumulative carbon emissions towards the trillionth tonne, Nature, 458, 1163–1166, 2009.

570 Arora, V. K., Katavouta, A., Williams, R. G., Jones, C. D., Brovkin, V., Friedlingstein, P., Schwinger, J., Bopp, L., Boucher, O., Cadule, P., Chamberlain, M. A., Christian, J. R., Delire, C., Fisher, R. A., Hajima, T., Ilyina, T., Joetzjer, E., Kawamiya, M., Koven, C. D., Krasting, J. P., Law, R. M., Lawrence, D. M., Lenton, A., Lindsay, K., Pongratz, J., Raddatz, T., Séférian, R., Tachiiri, K., Tjiputra, J. F., Wiltshire, A., Wu, T., and Ziehn, T.: Carbon–concentration and carbon–climate feedbacks in CMIP6 models and their comparison to CMIP5 models, https://doi.org/10.5194/bg-17-4173-2020, 2020.

575 Aumont, O., Ethé, C., Tagliabue, A., Bopp, L., and Gehlen, M.: PISCES-v2: an ocean biogeochemical model for carbon and ecosystem studies, Geosci. Model Dev., 8, 2465–2513, 2015.

Avis, C. A., Weaver, A. J., and Meissner, K. J.: Reduction in areal extent of high-latitude wetlands in response to permafrost thaw, Nat. Geosci., 4, 444–448, 2011.

Best, M. J., Pryor, M., Clark, D. B., Rooney, G. G., Essery, R. L. H., Ménard, C. B., Edwards, J. M., Hendry, M. A., Porson, 580 A., Gedney, N., Mercado, L. M., Sitch, S., Blyth, E., Boucher, O., Cox, P. M., Grimmond, C. S. B., and Harding, R. J.: The Joint UK Land Environment Simulator (JULES), model description – Part 1: Energy and water fluxes, Geosci. Model Dev., 4, 677–699, 2011.

Boucher, O., Denvil, S., Caubel, A., and Foujols, M. A.: IPSL IPSL-CM6A-LR model output prepared for CMIP6 CMIP

historical, https://doi.org/10.22033/ESGF/CMIP6.5195, 2018.

585 Boucher, O., Denvil, S., Caubel, A., and Foujols, M. A.: IPSL IPSL-CM6A-LR model output prepared for CMIP6 ScenarioMIP ssp534-over, https://doi.org/10.22033/ESGF/CMIP6.5269, 2019a.

Boucher, O., Denvil, S., Caubel, A., and Foujols, M. A.: IPSL IPSL-CM6A-LR model output prepared for CMIP6 ScenarioMIP ssp585, https://doi.org/10.22033/ESGF/CMIP6.5271, 2019b.

Boucher, O., Servonnat, J., Albright, A. L., Aumont, O., Balkanski, Y., Bastrikov, V., Bekki, S., Bonnet, R., Bony, S., Bopp, 590 L., Braconnot, P., Brockmann, P., Cadule, P., Caubel, A., Cheruy, F., Codron, F., Cozic, A., Cugnet, D., D'Andrea, F., Davini, P., Lavergne, C., Denvil, S., Deshayes, J., Devilliers, M., Ducharne, A., Dufresne, J., Dupont, E., Éthé, C., Fairhead, L., Falletti, L., Flavoni, S., Foujols, M., Gardoll, S., Gastineau, G., Ghattas, J., Grandpeix, J., Guenet, B., Guez, L. E., Guilyardi, E., Guimberteau, M., Hauglustaine, D., Hourdin, F., Idelkadi, A., Joussaume, S., Kageyama, M., Khodri, M., Krinner, G., Lebas, N., Levavasseur, G., Lévy, C., Li, L., Lott, F., Lurton, T., Luyssaert, S., Madec, G., Madeleine, J., Maignan, F., Marchand, 595 M., Marti, O., Mellul, L., Meurdesoif, Y., Mignot, J., Musat, I., Ottlé, C., Peylin, P., Planton, Y., Polcher, J., Rio, C., Rochetin, N., Rousset, C., Sepulchre, P., Sima, A., Swingedouw, D., Thiéblemont, R., Traore, A. K., Vancoppenolle, M., Vial, J., Vialard, J., Viovy, N., and Vuichard, N.: Presentation and evaluation of the IPSL-CM6A-LR climate model, J. Adv. Model. Earth Syst., 12, https://doi.org/10.1029/2019ms002010, 2020.

Clark, D. B., Mercado, L. M., Sitch, S., Jones, C. D., Gedney, N., Best, M. J., Pryor, M., Rooney, G. G., Essery, R. L. H., 600 Blyth, E., Boucher, O., Harding, R. J., Huntingford, C., and Cox, P. M.: The Joint UK Land Environment Simulator (JULES), model description -- Part 2: Carbon fluxes and vegetation dynamics, 4, 701–722, 2011.

Danabasoglu, G.: NCAR CESM2-WACCM model output prepared for CMIP6 CMIP historical, https://doi.org/10.22033/ESGF/CMIP6.10071, 2019a.

Danabasoglu, G.: NCAR CESM2-WACCM model output prepared for CMIP6 ScenarioMIP ssp534-over, 605 https://doi.org/10.22033/ESGF/CMIP6.10114, 2019b.

Danabasoglu, G.: NCAR CESM2-WACCM model output prepared for CMIP6 ScenarioMIP ssp585, https://doi.org/10.22033/ESGF/CMIP6.10115, 2019c.

Danabasoglu, G., Lamarque, J. -F, Bacmeister, J., Bailey, D. A., DuVivier, A. K., Edwards, J., Emmons, L. K., Fasullo, J., Garcia, R., Gettelman, A., Hannay, C., Holland, M. M., Large, W. G., Lauritzen, P. H., Lawrence, D. M., Lenaerts, J. T. M., 610 Lindsay, K., Lipscomb, W. H., Mills, M. J., Neale, R., Oleson, K. W., Otto-Bliesner, B., Phillips, A. S., Sacks, W., Tilmes, S., Kampenhout, L., Vertenstein, M., Bertini, A., Dennis, J., Deser, C., Fischer, C., Fox-Kemper, B., Kay, J. E., Kinnison, D., Kushner, P. J., Larson, V. E., Long, M. C., Mickelson, S., Moore, J. K., Nienhouse, E., Polvani, L., Rasch, P. J., and Strand, W. G.: The Community Earth System Model Version 2 (CESM2), J. Adv. Model. Earth Syst., 12, 106, 2020.

Eyring, V., Bony, S., Meehl, G. A., Senior, C. A., Stevens, B., Stouffer, R. J., and Taylor, K. E.: Overview of the Coupled 615 Model Intercomparison Project Phase 6 (CMIP6) experimental design and organization, Geosci. Model Dev., 9, 1937–1958, 2016.

Fisher, R. A. and Koven, C. D.: Perspectives on the future of Land Surface Models and the challenges of representing complex terrestrial systems, J. Adv. Model. Earth Syst., https://doi.org/10.1029/2018MS001453, 2020.

Gidden, M. J., Riahi, K., Smith, S. J., Fujimori, S., Luderer, G., Kriegler, E., van Vuuren, D. P., van den Berg, M., Feng, L., 620 Klein, D., Calvin, K., Doelman, J. C., Frank, S., Fricko, O., Harmsen, M., Hasegawa, T., Havlik, P., Hilaire, J., Hoesly, R., Horing, J., Popp, A., Stehfest, E., and Takahashi, K.: Global emissions pathways under different socioeconomic scenarios for use in CMIP6: a dataset of harmonized emissions trajectories through the end of the century, Geosci. Model Dev., 12, 1443–1475, 2019.

Good, P., Sellar, A., Tang, Y., Rumbold, S., Ellis, R., Kelley, D., and Kuhlbrodt, T.: MOHC UKESM1.0-LL model output
prepared for CMIP6 ScenarioMIP ssp534-over, https://doi.org/10.22033/ESGF/CMIP6.6397, 2019a.

Good, P., Sellar, A., Tang, Y., Rumbold, S., Ellis, R., Kelley, D., and Kuhlbrodt, T.: MOHC UKESM1.0-LL model output
prepared for CMIP6 ScenarioMIP ssp585, https://doi.org/10.22033/ESGF/CMIP6.6405, 2019b.

Harper, A. B., Cox, P. M., Friedlingstein, P., Wiltshire, A. J., Jones, C. D., Sitch, S., Mercado, L. M., Groenendijk, M.,
Robertson, E., Kattge, J., Bönisch, G., Atkin, O. K., Bahn, M., Cornelissen, J., Niinemets, Ü., Onipchenko, V., Peñuelas, J.,
Poorter, L., Reich, P. B., Soudzilovskaia, N. A., and van Bodegom, P.: Improved representation of plant functional types and
physiology in the Joint UK Land Environment Simulator (JULES v4.2) using plant trait information, Geosci. Model Dev., 9,
2415–2440, 2016.

Harper, A. B., Wiltshire, A. J., Cox, P. M., Friedlingstein, P., Jones, C. D., Mercado, L. M., Sitch, S., Williams, K., and Duran-
Rojas, C.: Vegetation distribution and terrestrial carbon cycle in a carbon-cycle configuration of JULES4.6 with new plant
functional types, Geosci. Model Dev. Discuss., 1–34, 2018.

Herrington, T. and Zickfeld, K.: Path independence of climate and carbon cycle response over a broad range of cumulative
carbon emissions, Earth Syst. Dyn., 5, 409–422, 2014.

Hoffman, F. M., Randerson, J. T., Arora, V. K., Bao, Q., Cadule, P., Ji, D., Jones, C. D., Kawamiya, M., Khatiwala, S., Lindsay,
K., Obata, A., Shevliakova, E., Six, K. D., Tjiputra, J. F., Volodin, E. M., and Wu, T.: Causes and implications of persistent
atmospheric carbon dioxide biases in Earth System Models, J. Geophys. Res. Biogeosci., 119, 141–162, 2014.

Hourdin, F., Rio, C., Grandpeix, J., Madeleine, J., Cheruy, F., Rochetin, N., Jam, A., Musat, I., Idelkadi, A., Fairhead, L.,
Foujols, M., Mellul, L., Traore, A., Dufresne, J., Boucher, O., Lefebvre, M., Millour, E., Vignon, E., Jouhaud, J., Diallo, F.
B., Lott, F., Gastineau, G., Caubel, A., Meurdesoif, Y., and Ghattas, J.: LMDZ6A: The atmospheric component of the IPSL
climate model with improved and better tuned physics, J. Adv. Model. Earth Syst., 12, e2019MS001892, 2020.

Hu, A., Van Roekel, L., Weijer, W., Garuba, O. A., Cheng, W., and Nadiga, B. T.: Role of AMOC in Transient Climate
Response to Greenhouse Gas Forcing in Two Coupled Models, https://doi.org/10.1175/JCLI-D-19-1027.1, 2020.

Hurtt, G. C., Chini, L., Sahajpal, R., Frolking, S., Bodirsky, B. L., Calvin, K., Doelman, J. C., Fisk, J., Fujimori, S., Klein
Goldewijk, K., Hasegawa, T., Havlik, P., Heinimann, A., Humpenöder, F., Jungclaus, J., Kaplan, J. O., Kennedy, J., Krisztin,
T., Lawrence, D., Lawrence, P., Ma, L., Mertz, O., Pongratz, J., Popp, A., Poulter, B., Riahi, K., Shevliakova, E., Stehfest, E.,
Thornton, P., Tubiello, F. N., van Vuuren, D. P., and Zhang, X.: Harmonization of global land use change and management
for the period 850–2100 (LUH2) for CMIP6, Geosci. Model Dev., 13, 5425–5464, 2020.

IPCC: Climate Change: The IPCC Scientific Assessment, edited by: J.T. Houghton, G. J. J. and Ephraums, J. J., Cambridge
University Press, Cambridge, Great Britain, New York, NY, USA and Melbourne, Australia, 1990.

Jones, C. D., Robertson, E., Arora, V., Friedlingstein, P., Shevliakova, E., Bopp, L., Brovkin, V., Hajima, T., Kato, E.,
Kawamiya, M., Liddicoat, S., Lindsay, K., Reick, C. H., Roelandt, C., Segschneider, J., and Tjiputra, J.: Twenty-First-Century
Compatible CO2 Emissions and Airborne Fraction Simulated by CMIP5 Earth System Models under Four Representative
Concentration Pathways, J. Clim., 26, 4398–4413, 2013.

Jones, C. D., Ciais, P., Davis, S. J., Friedlingstein, P., Gasser, T., Peters, G. P., Rogelj, J., van Vuuren, D. P., Canadell, J. G.,
Cowie, A., Jackson, R. B., Jonas, M., Kriegler, E., Littleton, E., Lowe, J. A., Milne, J., Shrestha, G., Smith, P., Torvanger, A.,
and Wiltshire, A.: Simulating the Earth system response to negative emissions, Environ. Res. Lett., 11, 095012, 2016.

Keller, D. P., Oschlies, A., and Eby, M.: A new marine ecosystem model for the University of Victoria Earth System Climate
Model, Geosci. Model Dev., 5, 1195–1220, 2012.

Koven, C. D., Lawrence, D. M., and Riley, W. J.: Permafrost carbon−climate feedback is sensitive to deep soil carbon decomposability but not deep soil nitrogen dynamics, 112, 3752–3757, 2015.

665 Kriegler, E., Bauer, N., Popp, A., Humpenöder, F., Leimbach, M., Strefler, J., Baumstark, L., Bodirsky, B. L., Hilaire, J., Klein, D., Mouratiadou, I., Weindl, I., Bertram, C., Dietrich, J.-P., Luderer, G., Pehl, M., Pietzcker, R., Piontek, F., Lotze-Campen, H., Biewald, A., Bonsch, M., Giannousakis, A., Kreidenweis, U., Müller, C., Rolinski, S., Schultes, A., Schwanitz, J., Stevanovic, M., Calvin, K., Emmerling, J., Fujimori, S., and Edenhofer, O.: Fossil-fueled development (SSP5): An energy and resource intensive scenario for the 21st century, Glob. Environ. Change, 42, 297–315, 2017.

670 Krinner, G., Viovy, N., de Noblet-Ducoudre, N., Ogee, J., Polcher, J., Friedlingstein, P., Ciais, P., Sitch, S., and Prentice, I. C.: A dynamic global vegetation model for studies of the coupled atmosphere-biosphere system, Global Biogeochem. Cycles, 19, GB1015, 2005.

Lawrence, D. M., Fisher, R. A., Koven, C. D., Oleson, K. W., Swenson, S. C., Bonan, G., Collier, N., Ghimire, B., Kampenhout, L., Kennedy, D., Kluzek, E., Lawrence, P. J., Li, F., Li, H., Lombardozzi, D., Riley, W. J., Sacks, W. J., Shi, 675 M., Vertenstein, M., Wieder, W. R., Xu, C., Ali, A. A., Badger, A. M., Bisht, G., Broeke, M., Brunke, M. A., Burns, S. P., Buzan, J., Clark, M., Craig, A., Dahlin, K., Drewniak, B., Fisher, J. B., Flanner, M., Fox, A. M., Gentine, P., Hoffman, F., Keppel-Aleks, G., Knox, R., Kumar, S., Lenaerts, J., Leung, L. R., Lipscomb, W. H., Lu, Y., Pandey, A., Pelletier, J. D., Perket, J., Randerson, J. T., Ricciuto, D. M., Sanderson, B. M., Slater, A., Subin, Z. M., Tang, J., Thomas, R. Q., Val Martin, M., and Zeng, X.: The Community Land Model Version 5: Description of New Features, Benchmarking, and Impact of Forcing 680 Uncertainty, J. Adv. Model. Earth Syst., 11, 4245–4287, 2019.

Liddicoat, S. K., Wiltshire, A. J., Jones, C. D., Arora, V. K., Brovkin, V., Cadule, P., Hajima, T., Lawrence, D. M., Pongratz, J., Schwinger, J., and Others: Compatible Fossil Fuel CO2 emissions in the CMIP6 Earth System Models' Historical and Shared Socioeconomic Pathway experiments of the 21st Century, J. Clim., 1–72, 2020.

MacDougall, A. H. and Knutti, R.: Projecting the release of carbon from permafrost soils using a perturbed parameter ensemble 685 modelling approach, Biogeosciences, 13, 2123–2136, 2016.

MacDougall, A. H., Avis, C. A., and Weaver, A. J.: Significant contribution to climate warming from the permafrost carbon feedback, Nat. Geosci., 5, 719–721, 2012.

MacDougall, A. H., Frölicher, T. L., Jones, C. D., Rogelj, J., Matthews, H. D., Zickfeld, K., Arora, V. K., Barrett, N. J., Brovkin, V., Burger, F. A., and Others: Is there warming in the pipeline? A multi-model analysis of the Zero Emissions 690 Commitment from CO 2, Biogeosciences, 17, 2987–3016, 2020.

Madec, G., Bourdallé-Badie, R., Bouttier, P.-A., Bricaud, C., Bruciaferri, D., Calvert, D., Chanut, J., Clementi, E., Coward, A., Delrosso, D., Ethé, C., Flavoni, S., Graham, T., Harle, J., Iovino, D., Lea, D., Lévy, C., Lovato, T., Martin, N., Masson, S., Mocavero, S., Paul, J., Rousset, C., Storkey, D., Storto, A., and Vancoppenolle, M.: NEMO ocean engine, https://doi.org/10.5281/ZENODO.3248739, 13 October 2017.

695 Ma, L., Hurtt, G. C., Chini, L. P., Sahajpal, R., Pongratz, J., Frolking, S., Stehfest, E., Klein Goldewijk, K., O'Leary, D., and Doelman, J. C.: Global rules for translating land-use change (LUH2) to land-cover change for CMIP6 using GLM2, Geosci. Model Dev., 13, 3203–3220, 2020.

Manabe, S. and Stouffer, R. J.: Multiple-century response of a coupled ocean-atmosphere model to an increase of atmospheric carbon-dioxide, J. Clim., 7, 5–23, 1994.

700 Marti, O., Braconnot, P., Dufresne, J.-L., Bellier, J., Benshila, R., Bony, S., Brockmann, P., Cadule, P., Caubel, A., Codron, F., de Noblet, N., Denvil, S., Fairhead, L., Fichefet, T., Foujols, M.-A., Friedlingstein, P., Goosse, H., Grandpeix, J.-Y., Guilyardi, E., Hourdin, F., Idelkadi, A., Kageyama, M., Krinner, G., Lévy, C., Madec, G., Mignot, J., Musat, I., Swingedouw, D., and Talandier, C.: Key features of the IPSL ocean atmosphere model and its sensitivity to atmospheric resolution, Clim.

Dyn., 34, 1–26, 2010.

705 Mathesius, S. and Zickfeld, K.: UVic ESCM simulations of historical period, SSP1-2.6, SSP5-3.4-OS, and SSP5-8.5, https://doi.org/10.5281/ZENODO.4663137, 2021.

Matthews, H. D., Gillett, N. P., Stott, P. A., and Zickfeld, K.: The proportionality of global warming to cumulative carbon emissions, Nature, 459, 829–832, 2009.

Matthews, H. D., Landry, J.-S., Partanen, A.-I., Allen, M., Eby, M., Forster, P. M., Friedlingstein, P., and Zickfeld, K.:
710 Estimating Carbon Budgets for Ambitious Climate Targets, 3, 69–77, 2017.

Meinshausen, M., Smith, S., Calvin, K., Daniel, J., Kainuma, M., Lamarque, J.-F., Matsumoto, K., Montzka, S., Raper, S., Riahi, K., Thomson, A., Velders, G., and van Vuuren, D. P.: The RCP greenhouse gas concentrations and their extensions from 1765 to 2300, Clim. Change, 109, 213–241, 2011.

Meinshausen, M., Nicholls, Z., Lewis, J., Gidden, M. J., Vogel, E., Freund, M., Beyerle, U., Gessner, C., Nauels, A., Bauer,
715 N., Canadell, J. G., Daniel, J. S., John, A., Krummel, P., Luderer, G., Meinshausen, N., Montzka, S. A., Rayner, P., Reimann, S., Smith, S. J., van den Berg, M., Velders, G. J. M., Vollmer, M., and Wang, H. J.: The shared socio-economic pathway (SSP) greenhouse gas concentrations and their extensions to 2500, Geoscientific Model Development, https://doi.org/10.5194/gmd-13-3571-2020, 2020.

Mengis, N., Keller, D. P., MacDougall, A. H., Eby, M., Wright, N., Meissner, K. J., Oschlies, A., Schmittner, A., MacIsaac,
720 A. J., Matthews, H. D., and Zickfeld, K.: Evaluation of the University of Victoria Earth System Climate Model version 2.10 (UVic ESCM 2.10), https://doi.org/10.5194/gmd-13-4183-2020, 2020.

Nakashiki, N., Kim, D.-H., Bryan, F. O., Yoshida, Y., Tsumune, D., Maruyama, K., and Kitabata, H.: Recovery of thermohaline circulation under CO2 stabilization and overshoot scenarios, Ocean Model., 15, 200–217, 2006.

Nicholls, Z. R., Gieseke, R., Lewis, J., Nauels, A., and Meinshausen, M.: Implications of non-linearities between cumulative
725 CO2 emissions and CO2-induced warming for assessing the remaining carbon budget, Environ. Res. Lett., 15, 074017, 2020a.

Nicholls, Z. R., Meinshausen, M., Lewis, J., Gieseke, R., Dommenget, D., Dorheim, K., Fan, C.-S., Fuglestvedt, J. S., Gasser, T., Golüke, U., Goodwin, P., Hartin, C., Hope, A. P., Kriegler, E., Leach, N. J., Marchegiani, D., McBride, L. A., Quilcaille, Y., Rogelj, J., Salawitch, R. J., Samset, B. H., Sandstad, M., Shiklomanov, A. N., Skeie, R. B., Smith, C. J., Smith, S., Tanaka, K., Tsutsui, J., and Xie, Z.: Reduced Complexity Model Intercomparison Project Phase 1: introduction and evaluation of
730 global-mean temperature response, https://doi.org/10.5194/gmd-13-5175-2020, 2020b.

Nijsse, F. J. M. M., Cox, P. M., and Williamson, M. S.: Emergent constraints on transient climate response (TCR) and equilibrium climate sensitivity (ECS) from historical warming in CMIP5 and CMIP6 models, https://doi.org/10.5194/esd-11-737-2020, 2020.

O'Neill, B. C., Kriegler, E., Riahi, K., Ebi, K. L., Hallegatte, S., Carter, T. R., Mathur, R., and van Vuuren, D. P.: A new
735 scenario framework for climate change research: the concept of shared socioeconomic pathways, Clim. Change, 122, 387–400, 2014.

O'Neill, B. C., Tebaldi, C., van Vuuren, D., Eyring, V., Friedlingstein, P., Hurtt, G., Knutti, R., Kriegler, E., Lamarque, J.-F., Lowe, J., Meehl, J., Moss, R., Riahi, K., and Sanderson, B. M.: The Scenario Model Intercomparison Project (ScenarioMIP) for CMIP6, https://doi.org/10.5194/gmd-2016-84, 2016.

740 Proistosescu, C. and Huybers, P. J.: Slow climate mode reconciles historical and model-based estimates of climate sensitivity, Sci Adv, 3, e1602821, 2017.

Randerson, J. T., Lindsay, K., Munoz, E., Fu, W., Moore, J. K., Hoffman, F. M., Mahowald, N. M., and Doney, S. C.: Multicentury changes in ocean and land contributions to the climate-carbon feedback: CARBON CYCLE FEEDBACKS TO 2300 IN CESM, Global Biogeochem. Cycles, 29, 744–759, 2015.

745 Riahi, K., van Vuuren, D. P., Kriegler, E., Edmonds, J., O'Neill, B. C., Fujimori, S., Bauer, N., Calvin, K., Dellink, R., Fricko, O., Lutz, W., Popp, A., Cuaresma, J. C., Kc, S., Leimbach, M., Jiang, L., Kram, T., Rao, S., Emmerling, J., Ebi, K., Hasegawa, T., Havlik, P., Humpenöder, F., Da Silva, L. A., Smith, S., Stehfest, E., Bosetti, V., Eom, J., Gernaat, D., Masui, T., Rogelj, J., Strefler, J., Drouet, L., Krey, V., Luderer, G., Harmsen, M., Takahashi, K., Baumstark, L., Doelman, J. C., Kainuma, M., Klimont, Z., Marangoni, G., Lotze-Campen, H., Obersteiner, M., Tabeau, A., and Tavoni, M.: The Shared Socioeconomic
750 Pathways and their energy, land use, and greenhouse gas emissions implications: An overview, Glob. Environ. Change, 42, 153–168, 2017.

Rogelj, J., Forster, P. M., Kriegler, E., Smith, C. J., and Séférian, R.: Estimating and tracking the remaining carbon budget for stringent climate targets, Nature, 571, 335–342, 2019.

Sanderson, B.: The role of prior assumptions in carbon budget calculations, https://doi.org/10.5194/esd-11-563-2020, 2020.

755 Sellar, A. A., Jones, C. G., Mulcahy, J. P., Tang, Y., Yool, A., Wiltshire, A., O'Connor, F. M., Stringer, M., Hill, R., Palmieri, J., Woodward, S., Mora, L., Kuhlbrodt, T., Rumbold, S. T., Kelley, D. I., Ellis, R., Johnson, C. E., Walton, J., Abraham, N. L., Andrews, M. B., Andrews, T., Archibald, A. T., Berthou, S., Burke, E., Blockley, E., Carslaw, K., Dalvi, M., Edwards, J., Folberth, G. A., Gedney, N., Griffiths, P. T., Harper, A. B., Hendry, M. A., Hewitt, A. J., Johnson, B., Jones, A., Jones, C. D., Keeble, J., Liddicoat, S., Morgenstern, O., Parker, R. J., Predoi, V., Robertson, E., Siahaan, A., Smith, R. S., Swaminathan,
760 R., Woodhouse, M. T., Zeng, G., and Zerroukat, M.: UKESM1: Description and Evaluation of the U.K. Earth System Model, J. Adv. Model. Earth Syst., 11, 4513–4558, 2019.

Sellar, A. A., Walton, J., Jones, C. G., Wood, R., Abraham, N. L., Andrejczuk, M., Andrews, M. B., Andrews, T., Archibald, A. T., Mora, L., Dyson, H., Elkington, M., Ellis, R., Florek, P., Good, P., Gohar, L., Haddad, S., Hardiman, S. C., Hogan, E., Iwi, A., Jones, C. D., Johnson, B., Kelley, D. I., Kettleborough, J., Knight, J. R., Köhler, M. O., Kuhlbrodt, T., Liddicoat, S.,
765 Linova-Pavlova, I., Mizielinski, M. S., Morgenstern, O., Mulcahy, J., Neininger, E., O'Connor, F. M., Petrie, R., Ridley, J., Rioual, J., Roberts, M., Robertson, E., Rumbold, S., Seddon, J., Shepherd, H., Shim, S., Stephens, A., Teixiera, J. C., Tang, Y., Williams, J., Wiltshire, A., and Griffiths, P. T.: Implementation of U.k. earth system models for CMIP6, J. Adv. Model. Earth Syst., 12, https://doi.org/10.1029/2019ms001946, 2020.

Sellers, P. J., Bounoua, L., Collatz, G. J., Randall, D. A., Dazlich, D. A., Los, S. O., Berry, J. A., Fung, I., Tucker, C. J., Field,
770 C. B., and Jensen, T. G.: Comparison of Radiative and Physiological Effects of Doubled Atmospheric CO2 on Climate, Science, 271, 1402–1406, 1996.

Swart, N. C., Cole, J. N. S., Kharin, V. V., Lazare, M., Scinocca, J. F., Gillett, N. P., Anstey, J., Arora, V., Christian, J. R., Jiao, Y., Lee, W. G., Majaess, F., Saenko, O. A., Seiler, C., Seinen, C., Shao, A., Solheim, L., von Salzen, K., Yang, D., Winter, B., and Sigmond, M.: CCCma CanESM5 model output prepared for CMIP6 CMIP historical,
775 https://doi.org/10.22033/ESGF/CMIP6.3610, 2019a.

Swart, N. C., Cole, J. N. S., Kharin, V. V., Lazare, M., Scinocca, J. F., Gillett, N. P., Anstey, J., Arora, V., Christian, J. R., Jiao, Y., Lee, W. G., Majaess, F., Saenko, O. A., Seiler, C., Seinen, C., Shao, A., Solheim, L., von Salzen, K., Yang, D., Winter, B., and Sigmond, M.: CCCma CanESM5 model output prepared for CMIP6 ScenarioMIP ssp534-over, https://doi.org/10.22033/ESGF/CMIP6.3694, 2019b.

780 Swart, N. C., Cole, J. N. S., Kharin, V. V., Lazare, M., Scinocca, J. F., Gillett, N. P., Anstey, J., Arora, V., Christian, J. R., Jiao, Y., Lee, W. G., Majaess, F., Saenko, O. A., Seiler, C., Seinen, C., Shao, A., Solheim, L., von Salzen, K., Yang, D., Winter, B., and Sigmond, M.: CCCma CanESM5 model output prepared for CMIP6 ScenarioMIP ssp585, https://doi.org/10.22033/ESGF/CMIP6.3696, 2019c.

Swart, N. C., Cole, J. N. S., Kharin, V. V., Lazare, M., Scinocca, J. F., Gillett, N. P., Anstey, J., Arora, V., Christian, J. R.,
785   Hanna, S., Jiao, Y., Lee, W. G., Majaess, F., Saenko, O. A., Seiler, C., Seinen, C., Shao, A., Sigmond, M., Solheim, L., von
        Salzen, K., Yang, D., and Winter, B.: The Canadian Earth System Model version 5 (CanESM5.0.3), Geoscientific Model
        Development, 12, 4823–4873, 2019d.

        Tang, Y., Rumbold, S., Ellis, R., Kelley, D., Mulcahy, J., Sellar, A., Walton, J., and Jones, C.: MOHC UKESM1.0-LL model
        output prepared for CMIP6 CMIP historical, https://doi.org/10.22033/ESGF/CMIP6.6113, 2019.

790   Tierney, J. E., Poulsen, C. J., Montañez, I. P., Bhattacharya, T., Feng, R., Ford, H. L., Hönisch, B., Inglis, G. N., Petersen, S.
        V., Sagoo, N., Tabor, C. R., Thirumalai, K., Zhu, J., Burls, N. J., Foster, G. L., Goddéris, Y., Huber, B. T., Ivany, L. C.,
        Kirtland Turner, S., Lunt, D. J., McElwain, J. C., Mills, B. J. W., Otto-Bliesner, B. L., Ridgwell, A., and Zhang, Y. G.: Past
        climates inform our future, Science, 370, https://doi.org/10.1126/science.aay3701, 2020.

        Tokarska, K. B. and Zickfeld, K.: The effectiveness of net negative carbon dioxide emissions in reversing anthropogenic
795   climate change, https://doi.org/10.1088/1748-9326/10/9/094013, 2015.

        Tokarska, K. B., Gillett, N. P., Weaver, A. J., Arora, V. K., and Eby, M.: The climate response to five trillion tonnes of carbon,
        Nat. Clim. Chang., 6, 851–855, 2016.

        Tokarska, K. B., Zickfeld, K., and Rogelj, J.: Path independence of carbon budgets when meeting a stringent global mean
        temperature target after an overshoot, Earths Future, 7, 1283–1295, 2019.

800   Wiltshire, A. J., Burke, E. J., Chadburn, S. E., Jones, C. D., Cox, P. M., Davies-Barnard, T., Friedlingstein, P., Harper, A. B.,
        Liddicoat, S., Sitch, S. A., and Zaehle, S.: JULES-CN: a coupled terrestrial Carbon-Nitrogen Scheme (JULES vn5.1), ,
        https://doi.org/10.5194/gmd-2020-205, 2020.

        Yool, A., Popova, E. E., and Anderson, T. R.: MEDUSA-2.0: an intermediate complexity biogeochemical model of the marine
        carbon cycle for climate change and ocean acidification studies, Geosci. Model Dev., 6, 1767–1811, 2013.

805   Zickfeld, K., Eby, M., Weaver, A. J., Alexander, K., Crespin, E., Edwards, N. R., Eliseev, A. V., Feulner, G., Fichefet, T.,
        Forest, C. E., Friedlingstein, P., Goosse, H., Holden, P. B., Joos, F., Kawamiya, M., Kicklighter, D., Kienert, H., Matsumoto,
        K., Mokhov, I. I., Monier, E., Olsen, S. M., Pedersen, J. O. P., Perrette, M., Philippon-Berthier, G., Ridgwell, A., Schlosser,
        A., Schneider Von Deimling, T., Shaffer, G., Sokolov, A., Spahni, R., Steinacher, M., Tachiiri, K., Tokos, K. S., Yoshimori,
        M., Zeng, N., and Zhao, F.: Long-Term Climate Change Commitment and Reversibility: An EMIC Intercomparison, J. Clim.,
810   26, 5782–5809, 2013.

        Zickfeld, K., MacDougall, A. H., and Matthews, H. D.: On the proportionality between global temperature change and
        cumulative CO 2 emissions during periods of net negative CO 2 emissions, Environ. Res. Lett., 11, 055006, 2016.

815

Figures
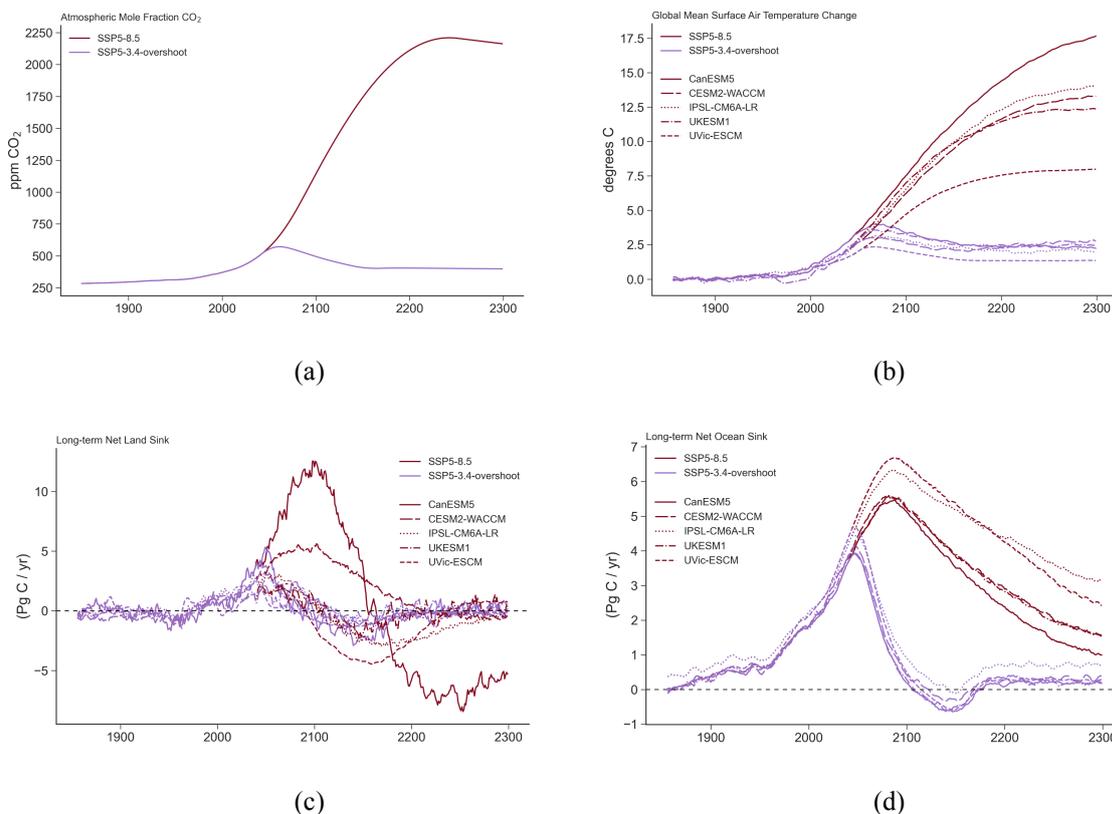
Fig. 1 (a) Atmospheric CO₂ concentrations for the high emissions SSP5-8.5 and mitigated SSP5-3.4-overshoot scenario out to 2300. (b) Global-mean surface air temperature. (c-d) Long term dynamics, as projected by 4 ESMs and 1 EMIC, of (c) the terrestrial carbon cycle, (d) the ocean carbon cycle, and, for both scenarios. All timeseries are smoothed to give 7-year running means, and positive flux represents a carbon sink into the land or ocean.

825

830
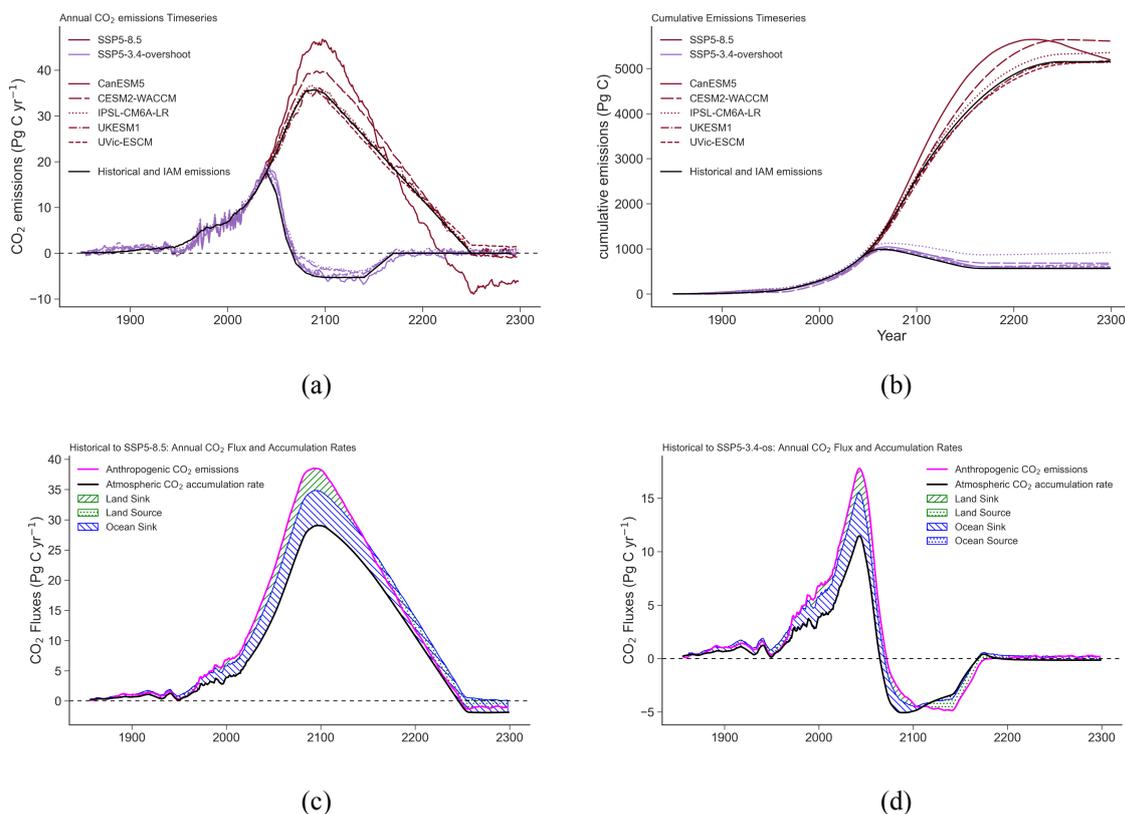
Fig. 2 (a) ESM-inferred and IAM-specified annual fossil-fuel (positive) and geologically sequesterred (negative) CO₂ emissions. (b) Cumulative fossil fuel (positive) and sequestration emissions (negative) as inferred by each ESM. (c-d) Ensemble-mean land, ocean, and emission fluxes shown together for the historical and future (c) SSP5-8.5 and (d) SSP5-3.4-overshoot scenarios. In (c-d), pink curves represent the annual CO₂ emissions, biospheric sink fluxes are represented as hatched area and source fluxes are represented as stippled area, and the atmospheric CO₂ accumulation, which is the sum of anthropogenic and biospheric fluxes, is shown as the black curve.
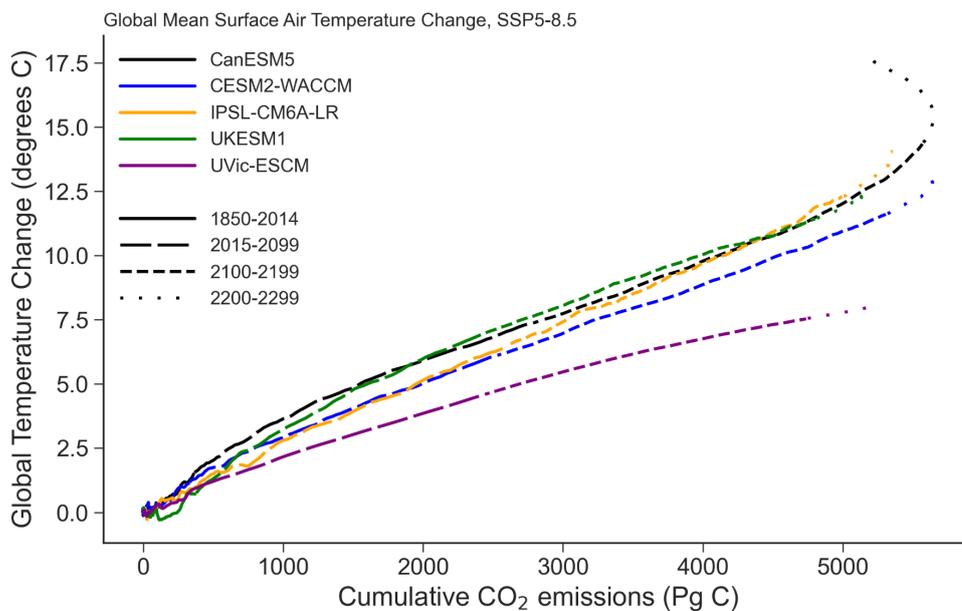
840   (a)
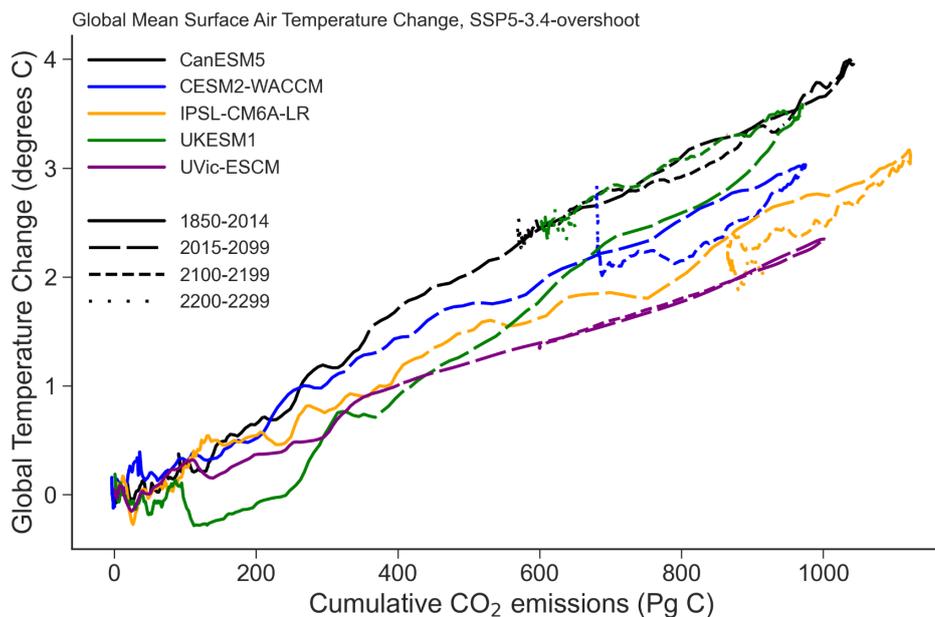
(b)

Fig. 3 Global warming as a function of cumulative emissions under the SSP5-8.5 (a) and SSP5-3.4-overshoot (b) scenarios. Each model is identified by a dash pattern, and the time period, broken into roughly centennial periods, are indicated by the color of the curves: historical (black), 21st century (green), 22nd century (blue), 23rd century (orange).

845
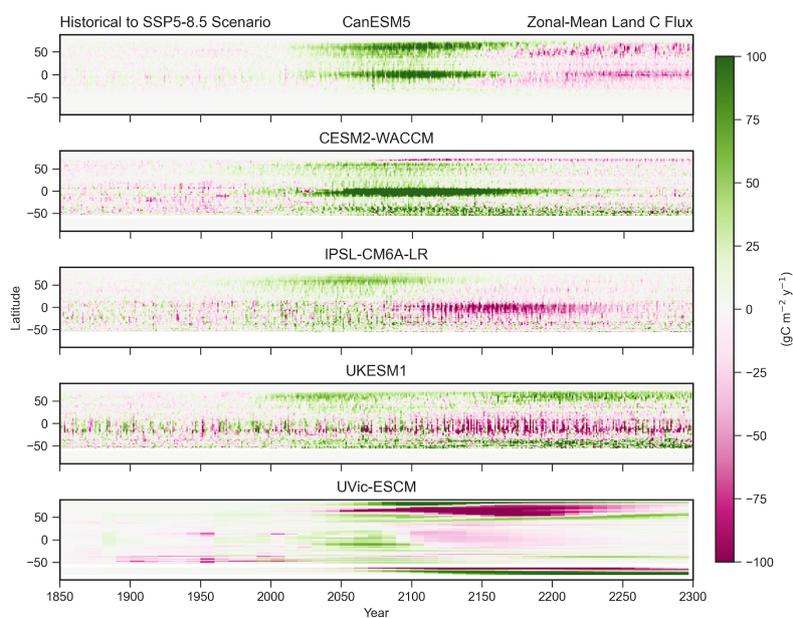
(a)
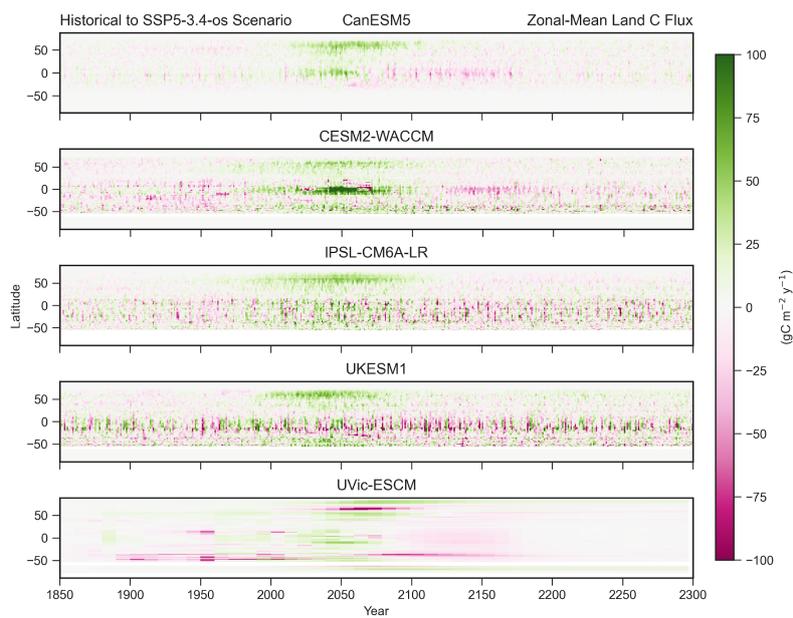
(b)

850   **Fig. 4 Zonal-mean terrestrial carbon flux dynamics of the five models under (a) the SSP5-8.5 and (b) SSP5-3.4-overshoot scenarios.**
       Positive flux represents a net carbon sink.
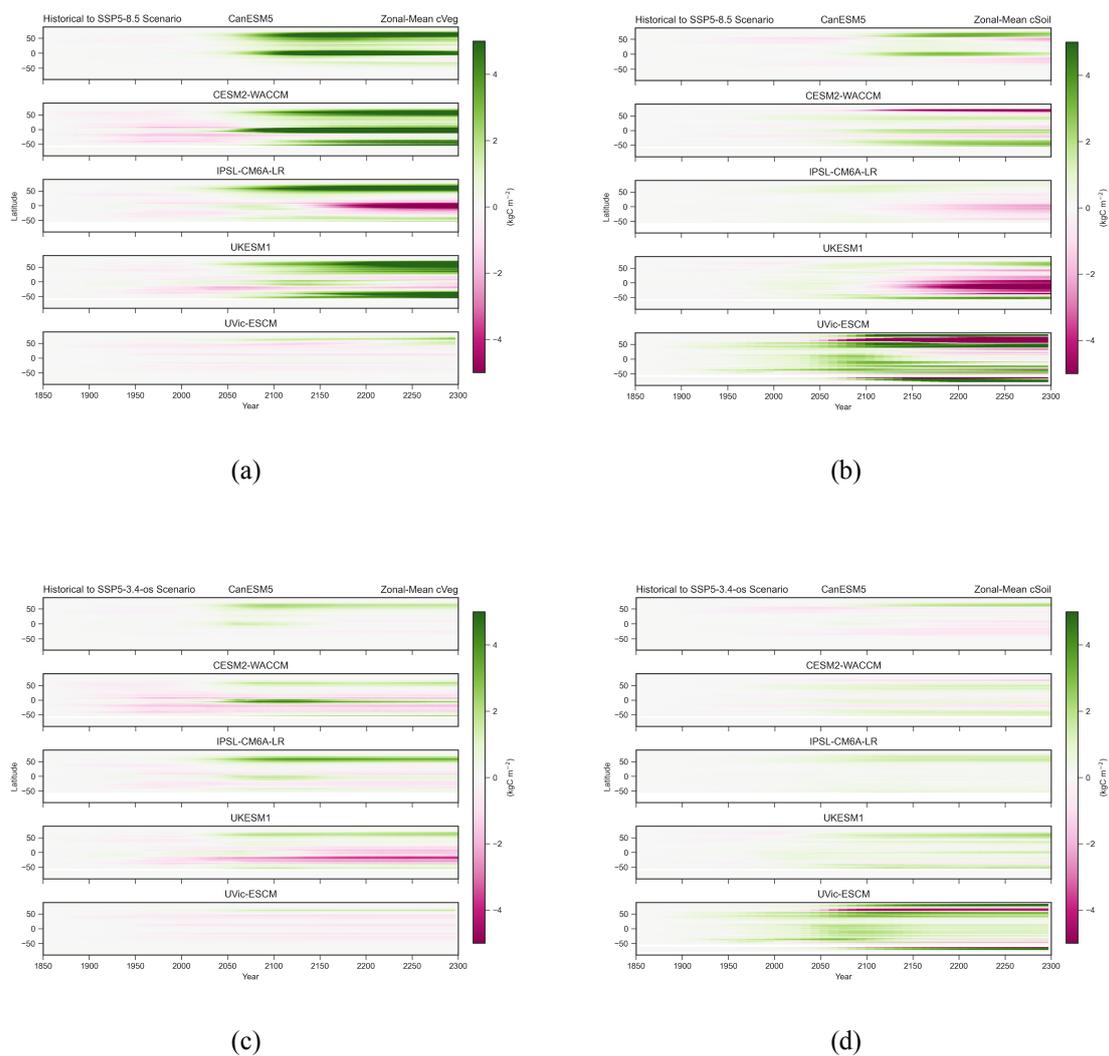
Fig. 5 Zonal-mean changes to terrestrial vegetation (left column) and soil carbon stocks (right column) in the five models for SSP5-8.5 and SSP5-3.4os scenarios (top and bottom rows, respectively).

(a)
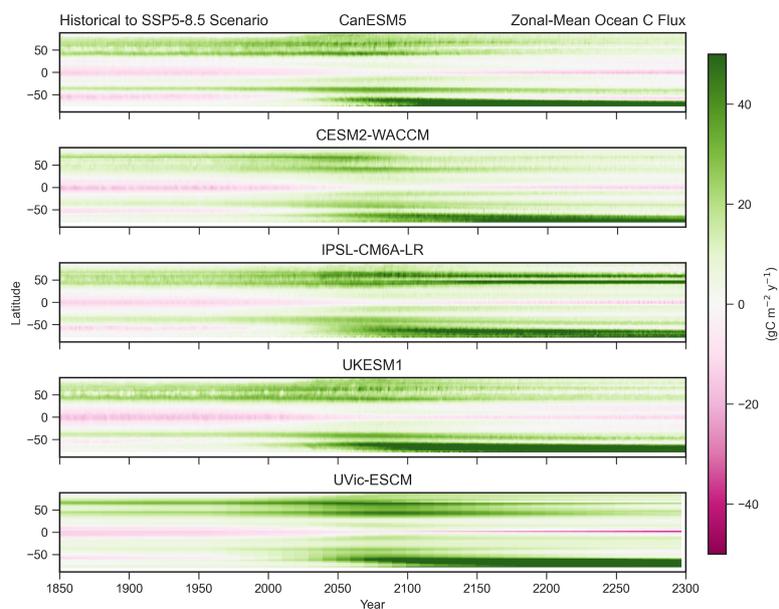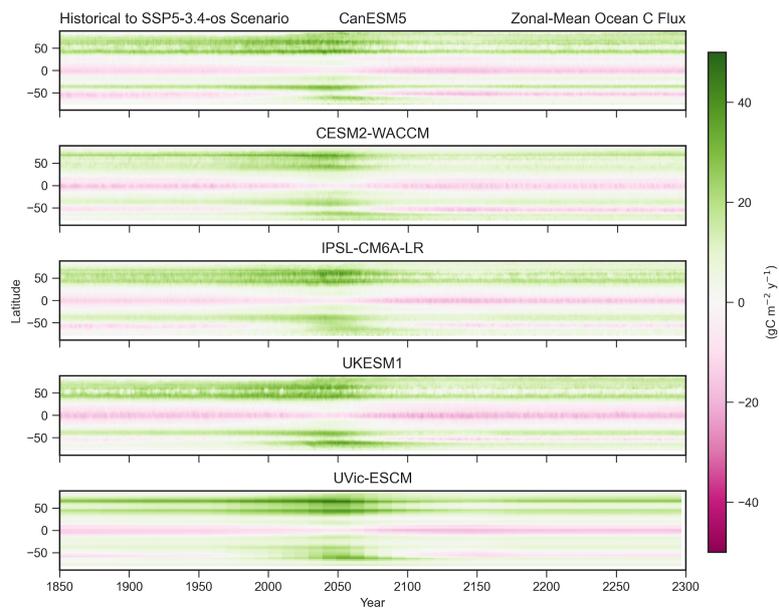
865   (b)

Fig. 6 Zonal-mean ocean carbon flux dynamics of the five models under (a) the SSP5-8.5 and (b) SSP5-3.4-overshoot scenarios. Positive flux represents a net carbon sink.

(a)

870
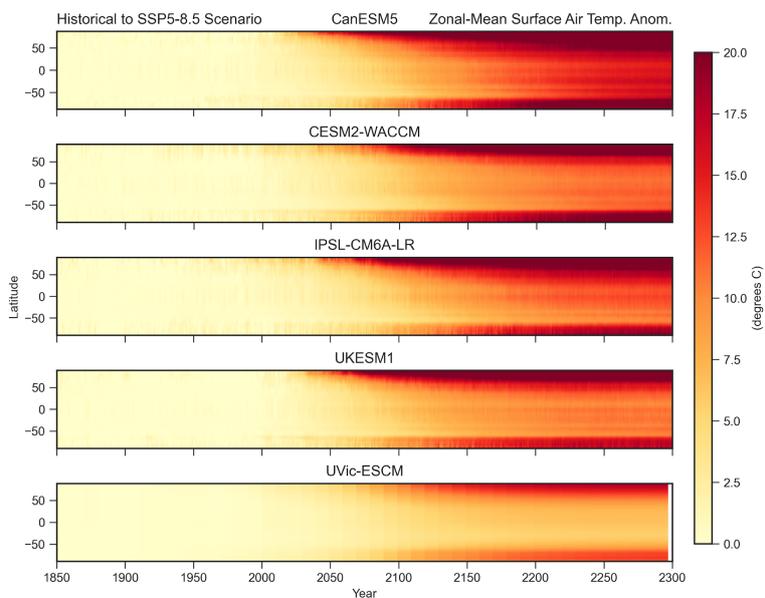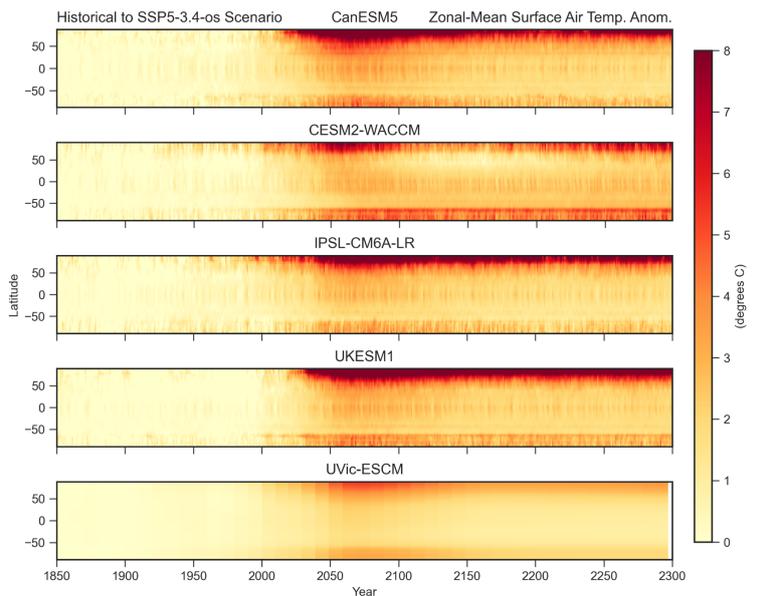
(b)

Fig. 7 Zonal-mean temperature anomaly timeseries of the five models under (a) the SSP5-8.5 and (b) SSP5-3.4-overshoot scenarios. Note the different color scales for each panel.
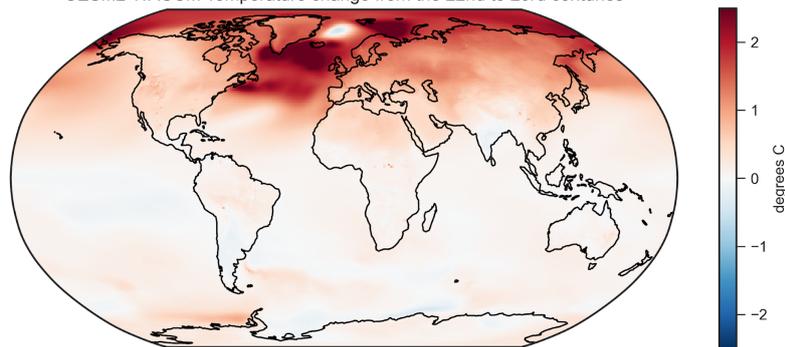
875

(a)
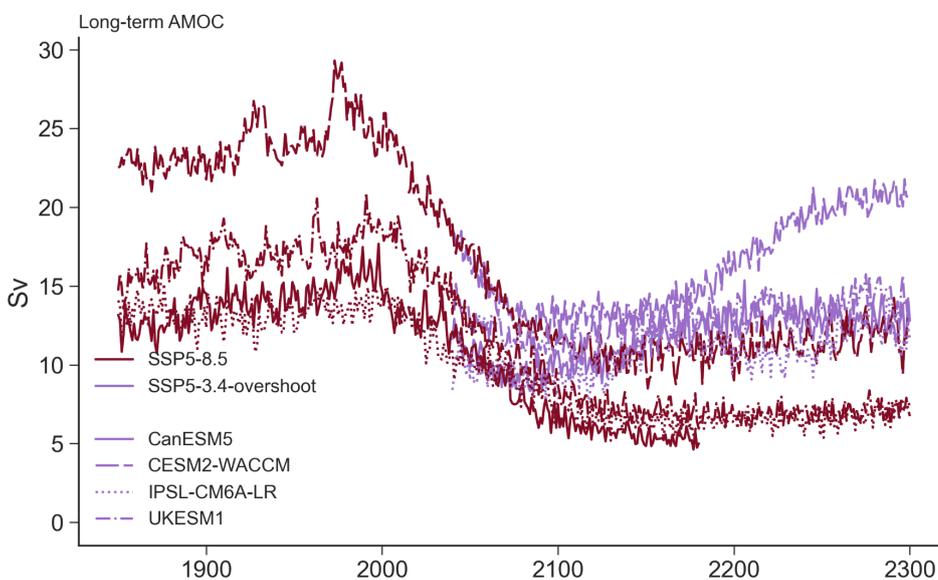
(b)

880   **Fig. 8 (a) Difference in the mean surface air temperature between the 22nd and 23rd centuries in the CESM2 model under the SSP5-3.4-overshoot. (b) Strength of the Atlantic Meridional Overturning Circulation for the all ESMs under both scenarios.**